

A Predictive Control Approach for Cooperative Transportation by Multiple Underwater Vehicle Manipulator Systems

Shahab Heshmati-Alamdar, George C. Karras and Kostas J. Kyriakopoulos

Abstract—This paper addresses the problem of cooperative object transportation for multiple Underwater Vehicle Manipulator Systems (UVMSs) in a constrained workspace involving static obstacles. We propose a Nonlinear Model Predictive Control (NMPC) approach for a team of UVMSs in order to transport an object while avoiding significant constraints and limitations such as: kinematic and representation singularities, obstacles within the workspace, joint limits and control input saturation. More precisely, by exploiting the coupled dynamics between the robots and the object, and using certain load sharing coefficients, we design a distributed NMPC for each UVMS in order to cooperatively transport the object within the workspace's feasible region. Moreover, the control scheme adopts load sharing among the UVMSs according to their specific payload capabilities. Additionally, the feedback relies on each UVMS's on-board measurements and no explicit data is exchanged online among the robots, thus reducing the required communication bandwidth. Finally, realistic simulation results conducted in UwSim dynamic simulator running in ROS environment as well as real time experiments performed within a test tank verify the effectiveness of the theoretical findings.

Index Terms—Underwater Vehicle Manipulator System, Cooperative Manipulation for Underwater Robots, Marine Robotics, Nonlinear Model Predictive Control, Underwater Navigation and Control.

I. INTRODUCTION

During the last decades, Unmanned Underwater Vehicles (UUVs) have been widely used in various applications such as marine science (e.g., biology, oceanography, archeology) and offshore industry (e.g., ship maintenance, inspection of oil/gas facilities) [1]. In particular, a vast number of the aforementioned applications, demand the underwater vehicle to be enhanced with intervention capabilities [2], hence raising the interest on Underwater Vehicle Manipulator System (UVMS) [3]. Nowadays, underwater intervention tasks involve a Remotely Operated Vehicle (ROV), equipped with one or multiple manipulators that allow it to grasp, transport and manipulate objects while being controlled by a human pilot on a surface ship, via a master-slave tele-operation scheme [4]–[6]. However, the well-known disadvantages of human-robot tele-operation (e.g., time delays, increase of human fatigue over time) led inevitably to the development of autonomous

Shahab Heshmati-alamdar is with the Division of Decision and Control Systems, School of Electrical Engineering and Computer Science, KTH Royal Institute of Technology, Stockholm, Sweden. G. C. Karras is with University of Thessaly, Lamia, Greece and with the Control Systems Lab, School of Mechanical Engineering, National Technical University of Athens, Greece. K. J. Kyriakopoulos are with the Control Systems Lab, School of Mechanical Engineering, National Technical University of Athens, Greece. Email: shaha@kth.se, {karrasg, kkyria@mail.ntua.gr}. (Corresponding author: Shahab Heshmati-alamdar)

This work was supported by the Knut och Alice Wallenberg Academy (KAW) Fellow 2015.0216.

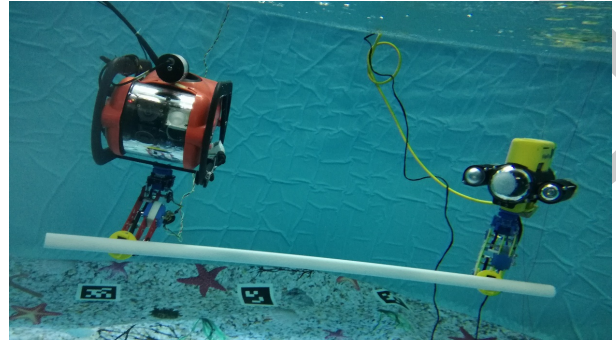


Fig. 1. Small custom made UVMSs under cooperative transportation in real time experimental study.

intervention control schemes for UVMS that have gained significant scientific attention during the last years [7], [8].

More specifically, during late 90s, early efforts towards designing underwater vehicle manipulator systems were made within the pioneering project AMADEUS [9], which was exploited later in both the UNION project [10] as well as the SAUVIM project [7], where for the first time autonomous underwater intervention was carried out. A more recent European project, which has boosted autonomous underwater interaction tasks, was the TRIDENT [11]–[16], where a vehicle-arm system was controlled in a coordinated manner. Another important milestone was achieved within the PANDORA project [17]–[19], where a strong emphasis was given on the problem of persistent autonomy. Finally, the most recent and related project in the domain of underwater intervention is the DexROV project [20], which focuses on inspection and maintenance tasks in the presence of communication latencies.

Most of the underwater manipulation tasks can be carried out more efficiently, if multiple UVMSs are cooperatively involved (see Fig. 1). For instance, two or more UVMSs can transport bulky objects more easily and safely than a single UVMS, owing to shape, actuation and payload constraints [21], [22]. In [21], the authors have studied the problem of modeling two UVMSs carrying a rigid object. The robot-object contact was considered rigid, thus the whole system configuration formed a singular system of differential equations [23]. The kinematic redundancy and manipulability of this system were examined in [24], [25]. Moreover, a centralized cooperative control scheme for multiple UVMSs holding commonly an object was proposed in [22]. However, in all aforementioned works, the major requirements and constraints imposed by the nature of underwater environment (e.g., limited communication, lack of appropriate sensing and localization) have not been considered at all.

Underwater multi-robot tasks are very demanding, with the most significant challenge being imposed by the strict commu-

nication constraints [7], [26]. In general, the communication of multi-robot systems can be classified in two major categories, namely explicit and implicit. The most investigated and frequently employed communication form in multi-robot systems is the explicit one. It usually leads to simpler theoretic analysis and renders teams more effective. However, even though the inter-robot communication is of utmost importance during cooperative manipulation tasks, employing explicit communication based control structure in underwater environment may result in severe performance problems owing to the limited bandwidth and update rate of underwater acoustic devices. Moreover, as the number of cooperating robots increases, communication protocols require complex design to deal with the crowded bandwidth [27]. Therefore, the number of operating underwater robots in this case, is strictly limited owing to the narrow bandwidth of acoustic communication devices. To overcome such limitations, recent studies on underwater cooperative manipulation are dealing with designing control schemes under lean communication requirements.

Cooperative manipulation has been well-studied in the literature, especially the centralized schemes [28]–[31]. Despite its efficiency, centralized control is less robust, since all units rely on a central system, and its complexity increases rapidly as the number of participating robots becomes large. On the other hand, although decentralized cooperative manipulation schemes exhibit increased robustness and low complexity, they usually depend on either explicit communication interchange among the robots (e.g., online transmission of the desired trajectory) [32]. For instance, in recent studies [33], [34], potential fields methods were employed and a multi layer control structure was developed to manage the guidance of UVMSs and the manipulation tasks. Moreover, interesting results towards the same direction have been given in [35]–[37], based on priority control strategy [38]. In particular, a three-fold decentralized cooperative control strategy is proposed where initially, each robot individually finds out an optimal task space control velocity, which is transferred afterwards among the robots in order to obtain a commonly agreed velocity via a fusion policy. The commonly agreed task velocity, is then extended to the joint space of each UVMS, based again on a task priority technique [38], but this time with a higher priority. Various safety constraints (e.g., joint limits, manipulability) may also be considered in case of two cooperating UVMSs. However, employing the aforementioned strategies, requires each robot to communicate with the whole team, which consequently restricts the number of robots involved in the cooperative manipulation task owing to bandwidth limitations.

Moreover, regarding cooperative manipulation, various studies can be found in the literature employing decentralized control schemes where robotic agents use only their local information or observation [31], [39], [40]. Most of the aforementioned studies assume that the robots are equipped with a force/torque sensor on their end effectors in order to acquire knowledge of the interaction contact forces/torques between the end effector and the common object, which may lead to a performance reduction due to sensor noise [41]–[43]. In addition, in most of the studies dealing with cooperative ma-

nipulation in literature, very important properties concerning the robotic manipulator systems such as: singular kinematic configurations of Jacobian matrix and joint limits have not been considered at all.

In this work, the problem of decentralized cooperative object transportation considering multiple UVMSs in a constrained workspace with static obstacles is addressed. Specifically, given N UVMSs rigidly grasp a common object, we design decentralized controllers for each UVMS in order to navigate the object from an initial position to the final one, while avoiding significant constraints and limitations such as: kinematic and representation singularities, obstacles within the workspace, joint limits and control input saturations. More precisely, by exploiting the coupled dynamics between the robots and the object and by using certain load sharing coefficients we design a distributed Nonlinear Model Predictive Control (NMPC) [44] for each UVMS in order to transport cooperatively the object and steer it along of a computed feasible path within the workspace. The design of that feasible path is based on the Navigation Function concept [45] which is adopted here in order to achieve distributed consensus on the object's desired trajectory as well to avoid collisions with the obstacles and the workspace boundary. In the proposed control strategy we also take into account constraints that emanate from control input saturation as well kinematic and representation singularities. Moreover, the control scheme adopts load sharing among the UVMSs according to their specific payload capabilities. In addition, it should be noticed that in the proposed methodology, each UVMS calculates its control signals without communicating with each other and exploits information acquired solely by onboard sensors, i.e., position and velocity measurements (e.g., sensor fusion based on measurement of various onboard sensors such as IMU, USBL and DVL), avoiding thus any tedious inter-robot explicit communication. This, consequently, increases significantly the robustness of the cooperative scheme and furthermore avoids any restrictions imposed by the acoustic communication bandwidth (e.g., the number of participating UVMSs). Finally, to the best of the authors knowledge and compared to the existing works in the literature, this is the first time where a cooperative manipulation scheme for multiple Underwater Vehicle Manipulator Systems is experimentally verified. Furthermore, it should be noticed that the proposed control strategy is more complete with respect to existing works, since it incorporates input (i.e., thrust saturation) and state (e.g., kinematic and representation singularities, 3D obstacles within the workspace, joint limits) constraints into the system's closed-loop motion while avoids any restrictions imposed by the strict underwater communication bandwidth.

The rest of the paper is organized as follows: In Section-II, the mathematical modeling along with the verbal description of the problem statement are presented. An analytical description of the proposed control method is presented in Section-III. The efficiency of the proposed approach is illustrated in Section-IV via both simulation and experimental studies. Finally, Section-V concludes the paper.

II. PROBLEM FORMULATION

Consider N UVMSs rigidly grasping an object¹ within a constrained workspace with static obstacles (see Fig 4). We also assume that each UVMS is fully-actuated at its end-effector frame. This assumption implies that all UVMSs are able to exert arbitrary forces and torques on the object along and about any direction. Moreover, we assume that the UVMSs are equipped with appropriate sensors, that allow them to measure their position and velocity (e.g., employing a sensor fusion technique based on measurements by various onboard sensors such as USBL, IMU, DVL and depth-sensor). Additionally, the geometric parameters of the both UVMSs and the commonly grasped object are considered known.

A. UVMS Kinematics

Consider N UVMSs operating in a bounded workspace $\mathcal{W} \subseteq \mathbb{R}^3$. First, we denote the coordinates of each UVMS's end effector by $\rho_i = [\eta_{1,p_i}^\top, \eta_{2,p_i}^\top]^\top$ where $\eta_{1,p_i}^\top = [x_{p_i}, y_{p_i}, z_{p_i}]^\top$ and $\eta_{2,p_i}^\top = [\phi_{p_i}, \theta_{p_i}, \psi_{p_i}]^\top$ denote the position and the orientation expressed in Euler angles with respect to the inertial frame. Let $q_i = [q_{B,i}^\top, q_{m,i}^\top]^\top \in \mathbb{R}^{n_i}$, with $n_i \in \mathbb{N}$, $i \in \mathcal{N}$ be the state variables of each UVMS, where $q_{B,i} = [\eta_{1,B_i}^\top, \eta_{2,B_i}^\top]^\top$ is the vector that involves the position η_{1,B_i}^\top and the orientation η_{2,B_i}^\top of the base and $q_{m,i}$ is the vector of the angular positions of the manipulator's joints. More specifically, $\eta_{1,B_i}^\top = [x_{B_i}, y_{B_i}, z_{B_i}]^\top$ and $\eta_{2,B_i}^\top = [\phi_{B_i}, \theta_{B_i}, \psi_{B_i}]^\top$, $i \in \{O, 1, \dots, N\}$ denote the position and the orientation expressed in Euler angles with respect to the inertial frame. Thus, we have [1], [46]:

$$\dot{q}_{B,i} = \mathbf{J}_{B,i}(q_{B,i})\rho_i, \quad i \in \mathcal{N} \quad (1)$$

where ρ_i is the velocity of the vehicle expressed in the body-fixed frame and $\mathbf{J}_{B,i}(q_{v,i})$ is the Jacobian matrix transforming the velocities from the body-fixed to the inertial frame. Let also define the UVMS' end effector generalized velocities by $v_i = [\dot{\eta}_{1,i}^\top, \omega_i^\top]^\top$, $i \in \mathcal{N}$, where $\dot{\eta}_{1,i}$ and ω_i denote the linear and angular velocity respectively. In addition, the position and orientation of the UVMS end-effector with respect to inertial frame, is given by the forward kinematics of the complete system (arm and vehicle base) as follows:

$$\rho_i = \mathcal{F}(q_i), \quad i \in \mathcal{N} \quad (2)$$

Moreover, without any loss of generality, for the augmented UVMS system we get [46]:

$$v_i = \mathbf{J}_i(q_i)\dot{q}_i, \quad i \in \mathcal{N} \quad (3)$$

where $\dot{q}_i = [\dot{q}_{B,i}^\top, \dot{q}_{m,i}^\top]^\top \in \mathbb{R}^{n_i}$ is the velocity vector involving the velocities of the vehicle with respect to the inertial frame as well as the joint velocities of the manipulator and $\mathbf{J}_i(q_i)$ is the geometric Jacobian matrix [46]. Note that the $\mathbf{J}_{B,i}$ becomes singular at representation singularities, when $\theta_{B_i} = \pm\frac{\pi}{2}$ and $\mathbf{J}_i(q_i)$ becomes singular at kinematic singularities defined by the set

$$Q_{s_i} = \{q_i \in \mathbb{R}^{n_i} : \det(\mathbf{J}_i(q_i)[\mathbf{J}_i(q_i)]^\top) \geq \epsilon\}, \quad i \in \mathcal{N}. \quad (4)$$

with ϵ to be a small positive number.

¹The end-effector frame of each UVMS is always constant relative to the object's body fixed frame.

B. UVMS Dynamics

Without any loss of generality, the dynamics of a UVMS after straightforward algebraic manipulations can be written as [46]:

$$\begin{aligned} \mathbf{M}_{q_i}(q_i)\ddot{q}_i + \mathbf{C}_{q_i}(\dot{q}_i, q_i)\dot{q}_i + \mathbf{D}_{q_i}(\dot{q}_i, q_i)\dot{q}_i + \mathbf{g}_{q_i}(q_i) = \\ \tau_i - \mathbf{J}_i^\top \lambda_i \end{aligned} \quad (5)$$

for $i \in \mathcal{N}$, where λ_i is the vector of generalized interaction forces and torques that UVMS exerts on the object, τ_i denotes the vector of control inputs (forces and torques), $\mathbf{M}_{q_i}(q_i)$ is the inertial matrix, $\mathbf{C}_{q_i}(\dot{q}_i, q_i)$ represents coriolis and centrifugal terms, $\mathbf{D}_{q_i}(\dot{q}_i, q_i)$ models dissipative effects and $\mathbf{g}_i(q_i)$ encapsulates the gravity and buoyancy effects. In view of (3) we have:

$$\dot{v}_i = \mathbf{J}_i(q_i)\ddot{q}_i + \dot{\mathbf{J}}_i(q_i)\dot{q}_i, \quad i \in \mathcal{N} \quad (6)$$

where $\dot{\mathbf{J}}_i(q_i) \in \mathbb{R}^{6 \times n_i}$ represents the Jacobian derivative function. Then, by employing the differential kinematics (3) as well as (6), we obtain from (5) the transformed task space dynamics [47]:

$$\mathbf{M}_i(q_i)\dot{v}_i + \mathbf{C}_i(\dot{q}_i, q_i)v_i + \mathbf{D}_i(\dot{q}_i, q_i)v_i + \mathbf{g}_i(q_i) = \mathbf{u}_i - \lambda_i \quad (7)$$

for all $i \in \mathcal{N}$ with corresponding task space terms $\mathbf{M}_i \in \mathbb{R}^{6 \times 6}$, $\mathbf{C}_i \in \mathbb{R}^{6 \times 6}$, $\mathbf{D}_i \in \mathbb{R}^{6 \times 6}$, $\mathbf{g}_i \in \mathbb{R}^6$:

$$\begin{aligned} \mathbf{M}_i(q_i) &= [\mathbf{J}_i(q_i)\mathbf{M}_{q_i}^{-1}\mathbf{J}_i(q_i)^\top]^{-1} \\ \mathbf{C}_i(\dot{q}_i, q_i)\mathbf{J}_i(q_i)\dot{q}_i &= \mathbf{M}_i(q_i)[\mathbf{J}_i(q_i)\mathbf{M}_{q_i}^{-1}\mathbf{C}_{q_i} - \dot{\mathbf{J}}_i(q_i)]\dot{q}_i \\ \mathbf{D}_i(\dot{q}_i, q_i)\mathbf{J}_i(q_i)\dot{q}_i &= \mathbf{M}_i(q_i)\mathbf{J}_i(q_i)\mathbf{M}_{q_i}^{-1}\mathbf{D}_{q_i}\dot{q}_i \\ \mathbf{g}_i(q_i) &= \mathbf{M}_i(q_i)\mathbf{J}_i(q_i)\mathbf{M}_{q_i}^{-1}\mathbf{g}_{q_i} \end{aligned}$$

Moreover, $\mathbf{u}_i \in \mathbb{R}^6$ is the vector of task space generalized forces/torques. It is worth noting that the vector of control inputs τ_i , $i \in \mathcal{K}$ can be related to the task space wrench $\mathbf{u}_i \in \mathbb{R}^6$, $i \in \mathcal{K}$ via:

$$\tau_i = \mathbf{J}_i^\top(q_i)\mathbf{u}_i + \tau_{i0}(q_i) \quad (8)$$

where the vector $\tau_{i0}(q_i)$ does not contribute to the end effector's wrench \mathbf{u}_i (i.e., it belongs to the null space of the Jacobian \mathbf{J}_i^\top) and can be regulated independently to achieve secondary tasks (e.g., maintaining manipulator's joint limits, increasing the manipulability) [47]². The UVMS task space dynamics (7) can be written in vector form as:

$$\mathbf{M}(q)\dot{v} + \mathbf{C}(\dot{q}, q)v + \mathbf{D}(\dot{q}, q)v + \mathbf{g}(q) = \mathbf{u} - \lambda \quad (9)$$

where $\mathbf{v} = [v_1^\top, \dots, v_N^\top]^\top \in \mathbb{R}^{6N}$, $\mathbf{M} = \text{diag}\{[\mathbf{M}_i]\} \in \mathbb{R}^{6N \times 6N}$, $\mathbf{C} = \text{diag}\{[\mathbf{C}_i]\} \in \mathbb{R}^{6N \times 6N}$, $\mathbf{D} = \text{diag}\{[\mathbf{D}_i]\} \in \mathbb{R}^{6N \times 6N}$, $\lambda = [\lambda_1^\top, \dots, \lambda_N^\top]^\top$, $\mathbf{u} = [u_1^\top, \dots, u_N^\top]^\top$, $\mathbf{g} = [g_1^\top, \dots, g_N^\top]^\top \in \mathbb{R}^{6N}$.

²For more details on task priority based control and redundancy resolution for UVMSs the reader is referred to [38] and [48].

C. Object Dynamics

We denote the coordinates of the object by $\mathbf{x}_O = [\eta_{1,O}^\top, \eta_{2,O}^\top]^\top$ where $\eta_{1,O}^\top = [x_O, y_O, z_O]^\top$ and $\eta_{2,O}^\top = [\phi_O, \theta_O, \psi_O]^\top$ denote the position and the orientation expressed in Euler angles with respect to the inertial frame. Let also define the object generalized velocities by $\mathbf{v}_O = [\dot{\eta}_{1,O}^\top, \omega_O^\top]^\top$. Without any loss of generality, we consider the following second order dynamics for the object, which can be derived based on the Newton-Euler formulations:

$$\dot{\mathbf{x}}_O = \mathbf{J}'_O(\eta_{2,O})^{-1} \mathbf{v}_O \quad (10a)$$

$$\mathbf{M}_O(\mathbf{x}_O) \ddot{\mathbf{v}}_O + \mathbf{C}_O(\mathbf{v}_O, \mathbf{x}_O) \mathbf{v}_O + \mathbf{D}_O(\mathbf{v}_O, \mathbf{x}_O) \mathbf{v}_O + \mathbf{g}_O = \boldsymbol{\lambda}_O \quad (10b)$$

where $\mathbf{M}_O(\mathbf{x}_O)$ is the positive definite inertia matrix, $\mathbf{C}_O(\mathbf{v}_O, \mathbf{x}_O)$ is the Coriolis matrix, \mathbf{g}_O is the vector of gravity and buoyancy effects, $\mathbf{D}_O(\mathbf{v}_O, \mathbf{x}_O)$ models dissipative effects and $\boldsymbol{\lambda}_O$ is the vector of generalized forces acting on the object's center of mass. Moreover, $\mathbf{J}'_O(\eta_{2,O})$ is the object representation Jacobian that transforms the Euler angle rates into velocity ω_O and can be given as:

$$\mathbf{J}'_O(\eta_{2,O}) = \begin{bmatrix} \mathbf{I}_3 & \mathbf{0}_{3 \times 3} \\ \mathbf{0}_{3 \times 3} & \mathbf{J}''_O(\eta_{2,O}) \end{bmatrix}, \quad (11)$$

with:

$$\mathbf{J}''_O(\eta_{2,O}) = \begin{bmatrix} 1 & 0 & -\sin(\theta_O) \\ 0 & \cos(\phi_O) & \cos(\theta_O) \sin(\phi_O) \\ 0 & -\sin(\phi_O) & \cos(\theta_O) \cos(\phi_O) \end{bmatrix}.$$

Note that the $\mathbf{J}'_O(\eta_{2,O})$ is singular when $\theta_O = \pm \frac{\pi}{2}$ [46].

D. Problem statement

Herein, we address the problem under consideration:

Problem 1: Given i) N UVMSs operating in a constrained workspace \mathcal{W} and rigidly grasping an object as well as ii) a desired configuration for the object \mathbf{x}_O^d , design distributed control protocols $\tau_i, i \in \mathcal{N}$ that navigate safely the whole robotic team to the desired configuration while satisfying the following specifications:

- 1) Collision avoidance with the obstacles and the boundary of the workspace;
- 2) Impose no strict requirements regarding the underwater communication bandwidth;
- 3) Avoiding the singular properties of the system;
- 4) Achieve distributed consensus on a mutually agreed trajectory of the commonly grasped object;

III. CONTROL METHODOLOGY

In this section we propose a solution to the Problem-1. The proposed approach builds on designing a Nonlinear Model Predictive Control scheme for the system of the UVMSs and the object. Thanks to the novel formulation of the problem, the proposed control strategy relieves the team of robots from intense inter-robot communication during the execution of the collaborative tasks which consequently reduces high bandwidth requirements. The control objective is to navigate of the overall formation towards the goal configuration while avoiding collisions with the static obstacles that lie within the workspace. First, the overall dynamics of the system (i.e.,

object and robots) are formulated accordingly. We achieve a decoupled form of the system dynamics by employing certain load coefficients. Each UVMS at each sampling time, solves a NMPC subject to its corresponding part of the overall dynamics and a number of inequality constraints that incorporate its internal limitations (e.g., joint limits, kinematic and representation singularities, collision between the arm and the base, manipulability) in order to guide cooperatively the object and steer it along a computed feasible path within the workspace. The feasible path computation is based on the concept of Navigation Functions [45] that is incorporated in order to deal with consensus on a mutually agreed trajectory of the commonly object.

Assumption 1: We assume that each UVMS $i \in \mathcal{N}$ is able to continuously measure its own state vector $\mathbf{q}_i, \dot{\mathbf{q}}_i, i \in \mathcal{N}$ based on its own state measurements (by employing sensor fusion of locally onboard navigation system sensors, e.g., DVL, IMU, USBL).

A. Coupled Dynamics

Consider the N UVMS rigidly grasping a common object. Owing to the rigid grasp of the object, the following equations hold:

$$\mathbf{p}_i = \mathbf{x}_O + \begin{bmatrix} {}^I \mathbf{R}_O \mathbf{l}_i \\ \boldsymbol{\alpha}_i \end{bmatrix}, \quad i \in \mathcal{N} \quad (12)$$

where the vectors $\mathbf{l}_i = [l_{ix}, l_{iy}, l_{iz}]^\top$ and $\boldsymbol{\alpha}_i = [\alpha_{ix}, \alpha_{iy}, \alpha_{iz}]^\top, i \in \mathcal{N}$ represent the *constant* relative position and orientation of the end-effector w.r.t the object, expressed in the object's frame and ${}^I \mathbf{R}_O$ denotes the rotation matrix which describes the orientation of the object expressed in the inertial frame $\{I\}$. Thus, using (12) each UVMS can compute the object's position w.r.t inertial frame $\{I\}$, since the object geometric parameters are considered known. Furthermore, due to the rigid grasp, it holds that $\omega_i = \omega_O, i \in \mathcal{N}$, hence we obtain:

$$\mathbf{v}_O = \mathbf{J}_{i_O} \mathbf{v}_i, \quad i \in \mathcal{N} \quad (13)$$

where $\mathbf{J}_{i_O}, i \in \mathcal{N}$ denotes the Jacobian from the end-effector of each UVMS to the object's center of mass, that is defined as:

$$\mathbf{J}_{i_O} = \begin{bmatrix} \mathbf{I}_{3 \times 3} & -\mathbf{S}(\mathbf{l}_i) \\ \mathbf{0}_{3 \times 3} & \mathbf{I}_{3 \times 3} \end{bmatrix} \in \mathbb{R}^{6 \times 6}, \quad i \in \mathcal{N}$$

where $\mathbf{S}(\mathbf{l}_i)$ is the skew-symmetric matrix of vector $\mathbf{l}_i = [l_{ix}, l_{iy}, l_{iz}]^\top$ defined as:

$$\mathbf{S}(\mathbf{l}_i) = \begin{bmatrix} 0 & -l_{iz} & l_{iy} \\ l_{iz} & 0 & -l_{ix} \\ -l_{iy} & l_{ix} & 0 \end{bmatrix} \in \mathbb{R}^{3 \times 3}, \quad i \in \mathcal{N}$$

Notice that $\mathbf{J}_{i_O}, i \in \mathcal{N}$ are always full-rank owing to the grasp rigidity and hence a well defined matrix inverse is obtained. Thus, the object's velocity can be easily computed via (13). Moreover, from (13), one obtains the acceleration relation:

$$\ddot{\mathbf{v}}_O = \mathbf{J}_{i_O} \ddot{\mathbf{v}}_i + \dot{\mathbf{J}}_{i_O} \mathbf{v}_i, \quad i \in \mathcal{N} \quad (14)$$

which will be used in the subsequent analysis. In addition, the kineto-statics duality along with the grasp rigidity suggest

that the force λ_O acting on the object's center of mass and the generalized forces λ_i , $i \in \mathcal{N}$, exerted by the UVMSs at the grasping points, are related through:

$$\lambda_O = \mathbf{G}^\top \boldsymbol{\lambda} \quad (15)$$

where:

$$\mathbf{G} = \left[[\mathbf{J}_{O_1}]^\top, \dots, [\mathbf{J}_{O_N}]^\top \right]^\top \in \mathbb{R}^{6N \times 6} \quad (16)$$

is the full column-rank grasp matrix, $\mathbf{J}_{O_i} = [\mathbf{J}_{i_O}]^{-1}$, $i \in \mathcal{N}$ and $\boldsymbol{\lambda} = [\lambda_1^\top, \dots, \lambda_N^\top]^\top$ is the vector containing the overall interaction forces and torques.

Remark 1: Wrenches that lie on the null space of the grasp matrix \mathbf{G}^\top do not contribute to the object dynamics. Therefore, we may incorporate in the control scheme an extra component $\lambda_{int,i} = (\mathbf{I} - (\mathbf{G}^\top)^\# \mathbf{G}^\top) \lambda_{int}^d$, $i \in \mathcal{N}$, that belongs to the null space of \mathbf{G}^\top , in order to regulate the steady state internal forces, where $(\mathbf{G}^\top)^\#$ denotes the generalized inverse of \mathbf{G}^\top . Notice that owing to the rigid grasp, l_i , $i \in \mathcal{N}$ remain constant. Thus, since l_i , $i \in \mathcal{N}$ are considered known to the team of UVMSs, if λ_{int}^d is chosen constant, no communication is needed during task execution in order to compute \mathbf{G}^\top , $(\mathbf{G}^\top)^\#$ and $\lambda_{int,i}$.

By substituting (9) into (15) one obtains:

$$\boldsymbol{\lambda} = \mathbf{G}^\top \left[\mathbf{u} - \mathbf{M}(\mathbf{q})\dot{\mathbf{v}} - \mathbf{C}(\dot{\mathbf{q}}, \mathbf{q})\mathbf{v} - \mathbf{D}(\dot{\mathbf{q}}, \mathbf{q})\mathbf{v} - \mathbf{g}(\mathbf{q}) \right] \quad (17)$$

which, after substituting (13), (14), (10) and rearranging terms, yields the overall system coupled dynamics:

$$\widetilde{\mathbf{M}}(\tilde{\mathbf{q}}_{ov})\dot{\mathbf{v}}_O + \widetilde{\mathbf{C}}(\tilde{\mathbf{q}}_{ov})\mathbf{v}_O + \widetilde{\mathbf{D}}(\tilde{\mathbf{q}}_{ov})\mathbf{v}_O + \widetilde{\mathbf{g}}(\tilde{\mathbf{q}}_{ov}) = \mathbf{G}^\top \mathbf{u} \quad (18)$$

where $\tilde{\mathbf{q}}_{ov} = [\mathbf{q}^\top, \dot{\mathbf{q}}^\top, \mathbf{x}_O^\top, \mathbf{v}_O^\top]^\top$ and:

$$\begin{aligned} \widetilde{\mathbf{M}}(\tilde{\mathbf{q}}_{ov}) &= \mathbf{M}_O(\mathbf{x}_O) + \mathbf{G}^\top \mathbf{M}(\mathbf{q})\mathbf{G} \\ \widetilde{\mathbf{C}}(\tilde{\mathbf{q}}_{ov}) &= \mathbf{C}_O(\mathbf{v}_O, \mathbf{x}_O) + \mathbf{G}^\top \mathbf{M}(\mathbf{q})\dot{\mathbf{G}}(\dot{\mathbf{q}}, \mathbf{q}) + \mathbf{G}^\top \mathbf{C}(\dot{\mathbf{q}}, \mathbf{q})\mathbf{G} \\ \widetilde{\mathbf{D}}(\tilde{\mathbf{q}}_{ov}) &= \mathbf{D}_O(\mathbf{v}_O, \mathbf{x}_O) + \mathbf{G}^\top \mathbf{D}(\dot{\mathbf{q}}, \mathbf{q})\mathbf{G} \\ \widetilde{\mathbf{g}}(\tilde{\mathbf{q}}_{ov}) &= \mathbf{g}_O(\mathbf{x}_O) + \mathbf{G}^\top \mathbf{g}(\mathbf{q}) \end{aligned}$$

Now, consider the design constants c_i , $i \in \mathcal{N}$ satisfying:

$$c_i \in (0, 1), \forall i \in \mathcal{N} \quad \text{and} \quad \sum_{i \in \mathcal{N}} c_i = 1, \quad (19)$$

which we introduce in order to act as the load sharing coefficients for the team of UVMS. In view of (19), the object dynamics (10b) can be rewritten as:

$$\sum_{i \in \mathcal{N}} c_i \left\{ \mathbf{M}_O(\mathbf{x}_O)\dot{\mathbf{v}}_O + \mathbf{C}_O(\mathbf{x}_O, \mathbf{v}_O)\mathbf{v}_O + \mathbf{D}_O(\mathbf{x}_O, \mathbf{v}_O)\mathbf{v}_O + \mathbf{g}_O(\mathbf{x}_O) \right\} = \sum_{i \in \mathcal{N}} \mathbf{J}_{O_i}^\top \boldsymbol{\lambda}_i \quad (20)$$

from which, by employing (3), (6), (13), (7) and (14), and after straightforward algebraic manipulations, we obtain the coupled dynamics:

$$\sum_{i \in \mathcal{N}} \left\{ \widetilde{\mathbf{M}}_i(\mathbf{q}_i)\ddot{\mathbf{q}}_i + \widetilde{\mathbf{C}}_i(\dot{\mathbf{q}}_i, \mathbf{q}_i)\dot{\mathbf{q}}_i + \widetilde{\mathbf{D}}_i(\dot{\mathbf{q}}_i, \mathbf{q}_i)\dot{\mathbf{q}}_i + \widetilde{\mathbf{g}}_i(\mathbf{q}_i) \right\} = \sum_{i \in \mathcal{N}} \mathbf{J}_{O_i}^\top \mathbf{u}_i \quad (21)$$

where:

$$\begin{aligned} \widetilde{\mathbf{M}}_i(\mathbf{q}_i) &= c_i \mathbf{M}_O \mathbf{J}_{i_O} \mathbf{J}_i + \mathbf{J}_{O_i}^\top \mathbf{M}_i \mathbf{J}_i \\ \widetilde{\mathbf{C}}_i(\dot{\mathbf{q}}_i, \mathbf{q}_i) &= \left\{ c_i \left[\mathbf{M}_O \mathbf{J}_{i_O} \dot{\mathbf{J}}_i + \mathbf{M}_O \dot{\mathbf{J}}_{i_O} \mathbf{J}_i + \mathbf{C}_O \mathbf{J}_{i_O} \mathbf{J}_i \right] + \mathbf{J}_{O_i}^\top \left[\mathbf{M}_i \dot{\mathbf{J}}_i + \mathbf{C}_i \mathbf{J}_i \right] \right\} \\ \widetilde{\mathbf{D}}_i(\dot{\mathbf{q}}_i, \mathbf{q}_i) &= c_i \mathbf{D}_O \mathbf{J}_{i_O} \mathbf{J}_i + \mathbf{J}_{O_i}^\top \mathbf{D}_i \mathbf{J}_i \\ \widetilde{\mathbf{g}}_i(\mathbf{q}_i) &= c_i \mathbf{g}_O + \mathbf{J}_{O_i}^\top \mathbf{g}_i \end{aligned}$$

which is the distributed version of (18), since for each UVMS, it is based only individually on its locally measurements (i.e., \mathbf{q}_i and $\dot{\mathbf{q}}_i$). Now, by using the notation $\mathbf{x}_i = [\mathbf{q}_i^\top, \dot{\mathbf{q}}_i^\top]^\top$, the individual dynamics for each UVMS based on (21), can be given in compact form:

$$\dot{\mathbf{x}}_i = f_i(\mathbf{x}_i, \mathbf{u}_i) = \begin{bmatrix} f_{i_1}(\mathbf{x}_i) \\ f_{i_2}(\mathbf{x}_i, \mathbf{u}_i) \end{bmatrix}, i \in \mathcal{N} \quad (22)$$

where:

$$\begin{aligned} f_{i_1}(\mathbf{x}_i) &= \dot{\mathbf{q}}_i \\ f_{i_2}(\mathbf{x}_i, \mathbf{u}_i) &= \widetilde{\mathbf{M}}_i^\#(\mathbf{q}_i) \left[\mathbf{J}_{O_i}^\top(\mathbf{q}_i) \mathbf{u}_i - \widetilde{\mathbf{C}}_i(\dot{\mathbf{q}}_i, \mathbf{q}_i) \dot{\mathbf{q}}_i - \widetilde{\mathbf{D}}_i(\dot{\mathbf{q}}_i, \mathbf{q}_i) \dot{\mathbf{q}}_i - \widetilde{\mathbf{g}}_i(\mathbf{q}_i) \right] \end{aligned}$$

with:

$$\widetilde{\mathbf{M}}_i^\#(\mathbf{q}_i) = \widetilde{\mathbf{M}}_i(\mathbf{q}_i) \left[\widetilde{\mathbf{M}}_i(\mathbf{q}_i) \widetilde{\mathbf{M}}_i^\top(\mathbf{q}_i) \right]^{-1}$$

B. Description of the Workspace

Consider the team of N UVMSs operating in a bounded workspace $\mathcal{W} \subseteq \mathbb{R}^3$ with boundary $\partial\mathcal{W}$. The object of interest is a rigid body which is required to be transported cooperatively by the robot team from an initial to a goal position. Without any loss of the generality, the obstacles, the robots as well as the workspace are all modeled by spheres (i.e., we adopt the spherical world representation [45]). In this spirit, let $\mathcal{B}(\mathbf{x}_O, r_0)$ be a closed sphere that covers the volume of the object and has radius r_0 . We also define the closed spheres $\mathcal{B}(\mathbf{p}_i, \bar{r})$, $i \in \mathcal{K}$, centered at the end-effector of each UVMS that cover the robot volume for all possible configurations. Notice that the value of \bar{r} can be calculated easily for each UVMS based solely on its own design parameters. We also assume that the distance among the grasping points on the given object is at least $2\bar{r}$. In particular, the distance $2\bar{r}$ denotes the minimum allowed distance at which two bounding spheres $\mathcal{B}(\mathbf{p}_i, \bar{r})$ and $\mathcal{B}(\mathbf{p}_j, \bar{r})$, $i, j \in \mathcal{K}$, $i \neq j$ do not collide (see Fig. 2). Furthermore, we define a sphere area $\mathcal{B}(\mathbf{x}_O, R)$ located at \mathbf{x}_O with radius $R = \bar{r} + r_o$ that includes the complete volume of the robotic team and the object (see Fig. 3). Finally, the \mathcal{M} static obstacles within the workspace are defined as closed spheres described by $\pi_m = \mathcal{B}(\mathbf{p}_{\pi_m}, r_{\pi_m})$, $m \in \{1, \dots, \mathcal{M}\}$, where $\mathbf{p}_{\pi_m} \in \mathbb{R}^3$ is the center and the $r_{\pi_m} > 0$ the radius of the obstacle π_m . Obviously, the ultimate goal of the proposed cooperative control strategy is to transport the object from the initial configuration to the desired one, without colliding

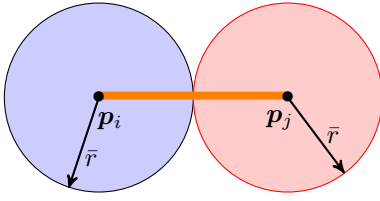


Fig. 2. Graphical representation of the minimum allowed distance $2\bar{r}$.

with the obstacles and the boundary of workspace. Therefore, based on the property of spherical world [45], for each pair of obstacles $m, m' \in \{1, \dots, \mathcal{M}\}$ the following inequality holds:

$$\|\mathbf{p}_{\pi_m} - \mathbf{p}_{\pi'_{m'}}\| > 2R + r_{\pi_m} + r_{\pi'_{m'}}$$

which intuitively means that the obstacles m and m' are disjoint in a such a way that the whole team of UVMSs including the object can pass through the free space between them. Therefore, there exists a feasible trajectory $\mathbf{x}_O(t)$ for the whole team that connects the initial configuration $\mathbf{x}_O(t_0)$ with \mathbf{x}_O^d such as:

$$\mathcal{B}(\mathbf{x}_O(t), R) \cap \{\mathcal{B}(\mathbf{p}_{\pi_m}, r_{\pi_m}) \cup \partial\mathcal{W}\} = \emptyset, \forall m \in \{1, \dots, \mathcal{M}\}$$

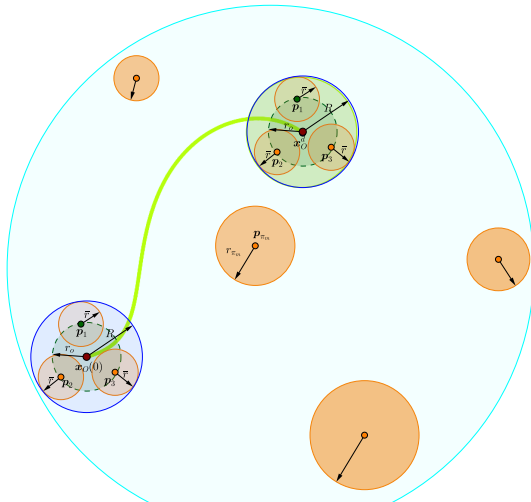


Fig. 3. Graphical representation of a safe trajectory of the robotic team. The boundary of workspace $\partial\mathcal{W}$ is illustrated in cyan. The orange areas indicate the obstacles within the workspace \mathcal{W} . The blue line encircles the area covered by the robotic team and the object. A safe trajectory of the whole team is depicted in green.

C. Safe Navigation

The desired object trajectory within the workspace \mathcal{W} relies on the Navigation Function concept originally proposed by Rimon and Koditschek in [45] as follows:

$$\phi_O(\mathbf{x}_O; \mathbf{x}_O^d) = \frac{\gamma(\mathbf{x}_O - \mathbf{x}_O^d)}{[\gamma^k(\mathbf{x}_O - \mathbf{x}_O^d) + \beta(\mathbf{x}_O)]^{\frac{1}{k}}} \quad (23)$$

where $\phi_O : \mathcal{W} - \bigcap_{m=1}^{\mathcal{M}} \mathcal{B}(\mathbf{p}_{\pi_m}, r_{\pi_m}) \rightarrow [0, 1]$ denotes the potential that derives a safe motion vector field within the free space $\mathcal{W} - \bigcap_{m=1}^{\mathcal{M}} \mathcal{B}(\mathbf{p}_{\pi_m}, r_{\pi_m})$. Moreover, $k > 1$ is a design constant,

$\gamma(\mathbf{x}_O - \mathbf{x}_O^d) > 0$ with $\gamma(\mathbf{0}) = 0$ represents the attractive potential field to the goal configuration \mathbf{x}_O^d and $\beta(\mathbf{x}_O) > 0$ with:

$$\lim_{\mathbf{x}_O \rightarrow \begin{cases} \text{Boundary} \\ \text{Obstacles} \end{cases}} \beta(\mathbf{x}_O) = 0$$

represents the repulsive potential field induced by the workspace boundary and the obstacle regions. In that respect, it was proven in [45] that $\phi_O(\mathbf{x}_O, \mathbf{x}_O^d)$ has a global minimum at \mathbf{x}_O^d and no other local minima for sufficiently large k . Thus, a feasible path that leads from any initial obstacle-free configuration³ to the desired configuration might be generated by following the negated gradient of $\phi_O(\mathbf{x}_O, \mathbf{x}_O^d)$. Consequently, the object's desired motion profile is designed as follows:

$$\dot{\mathbf{x}}_O^d(t) = -K_{NF} \mathbf{J}'_O(\eta_{2,O}) \nabla_{\mathbf{x}_O} \phi_O(\mathbf{x}_O(t), \mathbf{x}_O^d) \quad (24)$$

where $K_{NF} > 0$ is a positive gain. Now, let us define a sequence of sampling time $\{t_j\}_{j \geq 0}$ with a constant sampling time $h > 0$ with $h < T_p$ for the system such that:

$$t_{j+1} = t_j + h, \forall j \geq 0 \quad (25)$$

Therefore, since all UVMS $i \in \mathcal{N}$ are aware of both the desired configuration of the object as well as of the obstacles position in the workspace, given a current position of the object $\mathbf{x}_O(t_i)$ and $\mathbf{v}_O(t_j)$ at the time t_j they can propagate for time interval $s \in [t_j, t_j + T_p]$ where T_p is the prediction horizon, a map of desired trajectory and velocity of the object based on (23), (24) given as $\mathbf{x}_O^d(s)$ and $\mathbf{v}_O^d(s)$, $s \in [t_j, t_j + T_p]$ which will be used in the subsequent analysis.

D. Constraints

State Constraints:

In this work we assume that the UVMS must satisfy various constraints that can be considered as state constraints of the system. More specifically, joint limits and singularity avoidance should be satisfied by each UVMS. These requirements are captured by the state constraint set X_i of the system, given by:

$$\mathbf{x}_i(t) \in X_i \subset \mathbb{R}^{2n_i} \quad (26)$$

which is formed by the following constraints:

$$\theta_O(t) \in (-\frac{\pi}{2}, \frac{\pi}{2}) \quad (27)$$

$$\mathbf{q}_i \in \mathbb{R}^{n_i} \setminus (Q_{s_i}(\mathbf{q}_i) \cup Q_{l_i}(\mathbf{q}_i)), i \in \mathcal{N} \quad (28)$$

$$|\dot{q}_{k_i}| \leq \bar{q}_{k_i}, \forall k \in \{1, \dots, n\}, i \in \mathcal{N} \quad (29)$$

where $Q_{s_i}(\mathbf{q}_i)$ is the set of singular position of the system (4) and $Q_{l_i}(\mathbf{q}_i)$ is the set of manipulator's joint limits defined as:

$$Q_{l_i}(\mathbf{q}_i) = \{\mathbf{q}_i \in \mathbb{R}^{n_i} : |q_{k_i}| \leq \bar{q}_{k_i}\}, \forall k \in \{1, \dots, n_i\}, i \in \mathcal{N} \quad (30)$$

where \bar{q}_{k_i} is the limit bound for the corresponding joint q_{k_i} , $k \in \{1, \dots, n\}, i \in \mathcal{N}$. Moreover, \bar{q}_{k_i} is the upper value for the joint velocity \dot{q}_{k_i} , $k \in \{1, \dots, n\}, i \in \mathcal{N}$. Therefore, the set X_i captures all the state constraints of the systems (22), i.e., singularity avoidance as well as joint limits.

³Except from a set of measure zero [45].

Remark 2: Notice that collision avoidance between the complete system (UVMS and the object) and obstacles (see Fig 3) are achieved based on the desired trajectory and velocity of the object as calculated from (23) and (24).

Input Constraints:

The actuation of the vehicle and the manipulator are generated by the thrusters and servo motors respectively. Hence, the input constraints for τ_{k_i} , $k \in \{1, \dots, \tau_n\}$, $i \in \mathcal{N}$, with τ_n to be the number of actuated joints, can be given as:

$$\|\boldsymbol{\tau}_i\| \leq \bar{\boldsymbol{\tau}}_i \Leftrightarrow \|\mathbf{J}_i(\mathbf{q}_i)^\top \mathbf{u}_i\| \leq \bar{\boldsymbol{\tau}}_i$$

where $\bar{\boldsymbol{\tau}}_i$ is a vector including the corresponding limit bound for each actuated joint τ_{k_i} , $k \in \{1, \dots, \tau_n\}$, $i \in \mathcal{N}$. Therefore, we can define the control input set T_i :

$$\boldsymbol{\tau}_i(t) \in T_i \subset \mathbb{R}^{\tau_n} \quad (31)$$

with:

$$T_i = \{\boldsymbol{\tau}_i \in \mathbb{R}^{\tau_n} : \|\mathbf{J}_i(\mathbf{q}_i)^\top \mathbf{u}_i\| \leq \bar{\boldsymbol{\tau}}_i, \forall \mathbf{x}_i \in X_i\}$$

E. Control design

As it is already mentioned, given the current position and velocity of the object at sampling time j denoted by $\mathbf{x}_O(t_j)$ and $\mathbf{v}_O(t_j)$ respectively, each UVMS $i \in \mathcal{N}$ for a time interval $s \in [t_j, t_j + T_P]$ where T_P is a prediction horizon and based on (23), (24) and (25), can propagate a map of desired trajectory and velocity for the object denoted by $\mathbf{x}_O^d(s)$ and $\mathbf{v}_O^d(s)$ respectively. As it will be explained in the sequel, at each sampling time, UVMS $i \in \mathcal{N}$ solves its corresponding part of the dynamics (21) via an NMPC scheme subject to its dynamics (22) and a number of inequality constraints. More specifically, the control objective for each UVMS $i \in \mathcal{N}$ is to follow the desired trajectory and velocity, while respecting the state constraints (27)-(29) as well as the input constraints (31). In particular, in sampled data NMPC, a Finite Horizon Optimal Control Problem (FHOCP) is solved at discrete sampling time instants t_j based on the current state measurements $\mathbf{x}_i(t_j)$, $i \in \mathcal{N}$. For UVMS i , $i \in \mathcal{N}$, the open-loop input signal applied in between the sampling instants is given by the solution of the following FHOCP:

$$\min_{\hat{\boldsymbol{\tau}}_i(\cdot)} J_i(\mathbf{x}(t_j), \hat{\boldsymbol{\tau}}_i(\cdot)) = \quad (32a)$$

$$\begin{aligned} & \min_{\hat{\boldsymbol{\tau}}_i(\cdot)} \left\{ \int_{t_j}^{t_j+T_P} \left[F_i(\hat{\mathbf{x}}_O(s), \hat{\mathbf{v}}_O(s), \hat{\boldsymbol{\tau}}_i(s)) \right] ds \right. \\ & \quad \left. + E_i(\hat{\mathbf{x}}_O(t_j + T_P), \hat{\mathbf{v}}_O(t_j + T_P)) \right\} \end{aligned}$$

subject to:

$$\hat{\mathbf{x}}_i(s) = f_i(\hat{\mathbf{x}}_i(s), \hat{\mathbf{u}}_i(s)), \quad \hat{\mathbf{x}}_i(t_j) = \mathbf{x}_i(t_j), \quad (32b)$$

$$\hat{\boldsymbol{\tau}}_i(s) = \mathbf{J}_i^\top(\hat{\mathbf{q}}_i) \hat{\mathbf{u}}_i + \boldsymbol{\tau}_{i0}(\mathbf{q}_i), \quad s \in [t_j, t_j + T_P] \quad (32c)$$

$$\hat{\mathbf{x}}_O(s) = \mathcal{F}(\hat{\mathbf{q}}_i(s)) - \begin{bmatrix} {}^I\mathbf{R}_{OL} \\ \boldsymbol{\alpha}_i \end{bmatrix}, \quad s \in [t_j, t_j + T_P], \quad (32d)$$

$$\hat{\mathbf{v}}_O(s) = \mathbf{J}_{i0} \mathbf{J}_i(\hat{\mathbf{q}}_i(s)) \hat{\mathbf{q}}_i(s), \quad s \in [t_j, t_j + T_P], \quad (32e)$$

$$\hat{\mathbf{x}}_i(s) \in X_i, \quad s \in [t_j, t_j + T_P], \quad (32f)$$

$$\hat{\boldsymbol{\tau}}_i(s) \in T_i, \quad s \in [t_j, t_j + T_P], \quad (32g)$$

$$\hat{\mathbf{x}}(t_j + T_P) \in \mathcal{E}_f \quad (32h)$$

where \mathcal{E}_f is a terminal region around the desired trajectory profile. F and E are the running and terminal cost function respectively which are both of quadratic form i.e., $F(\cdot) = \hat{\mathbf{x}}_O^\top \mathbf{Q}_x \hat{\mathbf{x}}_O + \hat{\mathbf{v}}_O^\top \mathbf{Q}_v \hat{\mathbf{v}}_O + \boldsymbol{\tau}_i^\top \mathbf{R} \boldsymbol{\tau}_i$ and $E(\cdot) = \hat{\mathbf{x}}_O^\top \mathbf{P}_x \hat{\mathbf{x}}_O$, respectively, with \mathbf{P}_x , \mathbf{Q}_x , \mathbf{Q}_v and \mathbf{R} being positive definite matrices to be appropriately tuned [49]. In order to distinguish the predicted variables (i.e., internal to the controller) we use the double subscript notation (\cdot) corresponding to the system (32b). This means that $\hat{\mathbf{x}}_i(s)$, $s \in [t_j, t_j + T_P]$ is the solution of (22) based on the measurement of the state at time instance t_j (i.e., $\mathbf{x}_i(t_j)$, provided by the on-board navigation system) while applying a trajectory of inputs (i.e., $\hat{\mathbf{u}}_i(s)$, $s \in [t_j, t_j + T_P]$). The solution of FHOCP (32a)-(32h) at time t_j provides an optimal control input trajectory denoted by $\hat{\boldsymbol{\tau}}_i^*(s; \mathbf{x}(t_j))$, $s \in [t_j, t_j + T_P]$. This control input is then applied to the system until the next sampling time t_{j+1} :

$$\boldsymbol{\tau}_i(s; \mathbf{x}(t_j)) = \hat{\boldsymbol{\tau}}_i^*(s; \mathbf{x}(t_j)), \quad s \in [t_j, t_j + h] \quad (33)$$

At time $t_{j+1} = t_j + h$ a new finite horizon optimal control problem is solved in the same manner, leading to a receding horizon approach. Notice that the control input $\boldsymbol{\tau}_i(\cdot)$ is of feedback form, since it is recalculated at each sampling instant based on the then-current state. The pseudo-code description of the proposed real-time control scheme for UVMS i , $i \in \mathcal{N}$ is given in *Algorithm 1*:

Algorithm 1 Real time MPC algorithm:

- 1: **Triggering time** ▷ At time instance t_j UVMS i measures its state vector \mathbf{x}_i
 - 2: $\mathbf{p}_i(t_j) \leftarrow \text{eq.(2)}$ ▷ calculates its EE pose
 - 3: $\mathbf{v}_i(t_j) \leftarrow \text{eq.(3)}$ ▷ calculates its EE velocity
 - 4: $\mathbf{v}_O(t_j), \mathbf{x}_O(t_j) \leftarrow \text{eq.(12) - (13)}$ ▷ calculates object pose and velocity
 - 5: $\mathbf{x}_O^d(s), \mathbf{v}_O^d(s), s \in [t_j, t_j + T_P] \leftarrow \text{eq.(23), (24)}$ ▷ propagating for the time interval s , $s \in [t_j, t_j + T_P]$ a map of safe/desired trajectory and velocity of the object
 - 6: $\hat{\boldsymbol{\tau}}_i^*(s; \mathbf{x}(t_j)), s \in [t_j, t_j + T_P] \leftarrow \text{FHOCP}(\mathbf{x}_i(t_j))$ ▷ Run FHOCP of (32a)-(32h). The solution is an optimal control input trajectory for the time interval $[t_j, t_j + T_P]$.
 - 7: **for** $s \in [t_j, t_j + h]$ **do**
 - 8: Apply the $\boldsymbol{\tau}_i(s; \mathbf{x}(t_j)) = \hat{\boldsymbol{\tau}}_i^*(s; \mathbf{x}(t_j))$ to the UVMS.
 - 9: $t_{j+1} = t_j + h$ ▷ The next triggering time
 - 10: **goto** Triggering.
-

IV. RESULTS

In this section, the theoretical findings are verified via both simulation and experimental studies. The simulation results were conducted using a dynamic simulation environment based on the UwSim simulator [50] running on the Robot Operating System (ROS) [51]. The experimental results were conducted in a test tank employing two small UVMSs with in-house built underwater manipulators.

A. Simulation study

We consider a scenario involving 3D motion with two UVMSs with the same structure, transporting a bar-shaped

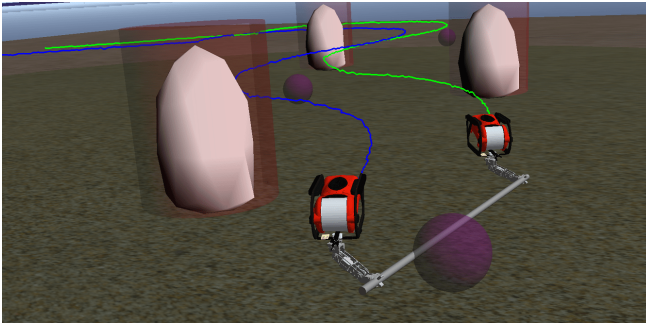


Fig. 4. Simulation environment: Cooperatively object transportation using two UVMSs inside a constrained workspace including obstacles.

object in a constrained workspace with static obstacles (see Fig.4). The UVMS model is a underwater robotic vehicle equipped with a small 4 DoF manipulator attached at the bow of the vehicle (see Fig.4). The dynamic parameters of the vehicle have been identified via a proper identification scheme [52], while the manipulator's parameters as well as object's parameters have been extrapolated by the CAD data. The complete state vector of the vehicle (3D position, orientation, velocity) is available via the sensor fusion and state estimation module given in our previous results [52]. The Constrained NMPC employed in this work is implemented using the NLOpt Optimization library [53].

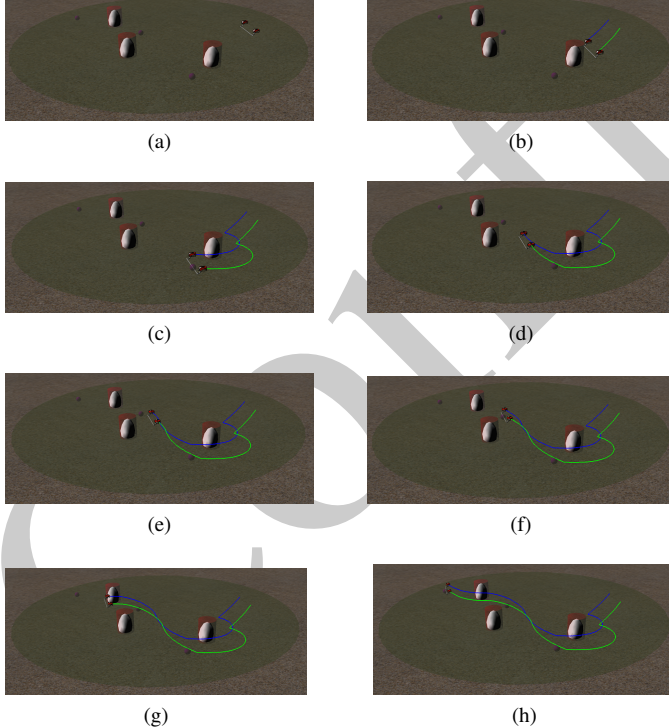


Fig. 5. Simulation study: the evolution of the proposed methodology in 8 consecutive time instants.

In the following simulation, the objective for the team of UVMSs is to follow a set of predefined way points, while simultaneously avoid obstacles within the workspace. The position of the obstacles w.r.t the inertial frame \mathcal{I} in $x - y$

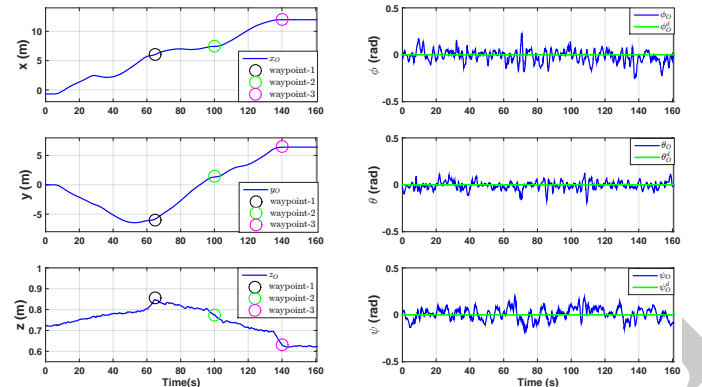


Fig. 6. Simulation study: object coordinates during the control operation

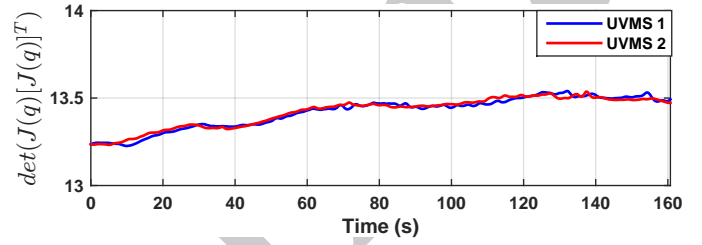


Fig. 7. Simulation study: $\det(\mathbf{J}(\mathbf{q})[\mathbf{J}(\mathbf{q})]^\top)$ during the control operation

plane is given by: $\mathbf{x}_{obs_1} = [4, -4.5]$, $\mathbf{x}_{obs_2} = [9, -1.5]$ and $\mathbf{x}_{obs_3} = [9, 5]$ respectively. These obstacles are cylinders with radius $r_{\pi_i} = 0.6m$, $i = \{1, 2, 3\}$ and are modeled together with the workspace boundaries according to the spherical world representations as consecutive spheres. The radius of the sphere $B(p_i, \bar{r})$, $i \in \{1, 2\}$ which covers all the UVMS volume (for all possible configurations) is defined as $\bar{r} = 1m$. In this way, the Navigation function (23)-(24) was designed with gain $K_{NF} = 0.5$. According to constraints (29), we

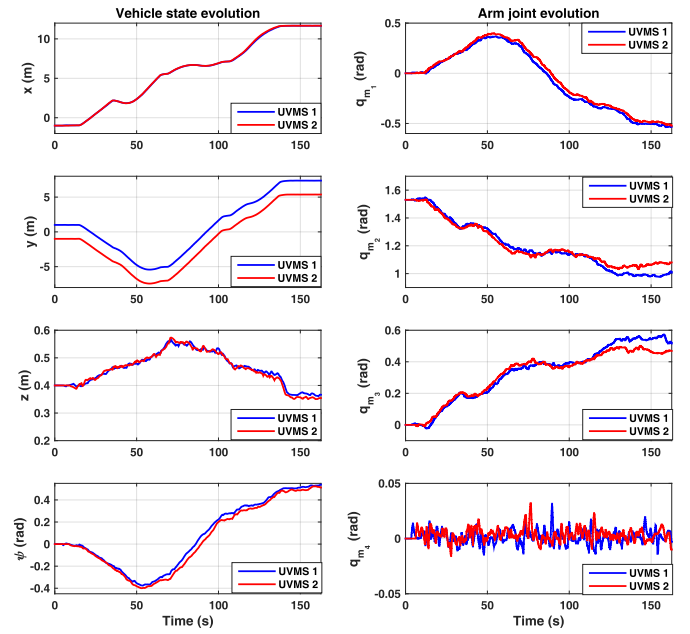


Fig. 8. Simulation study: the evolution of the system states at joint level

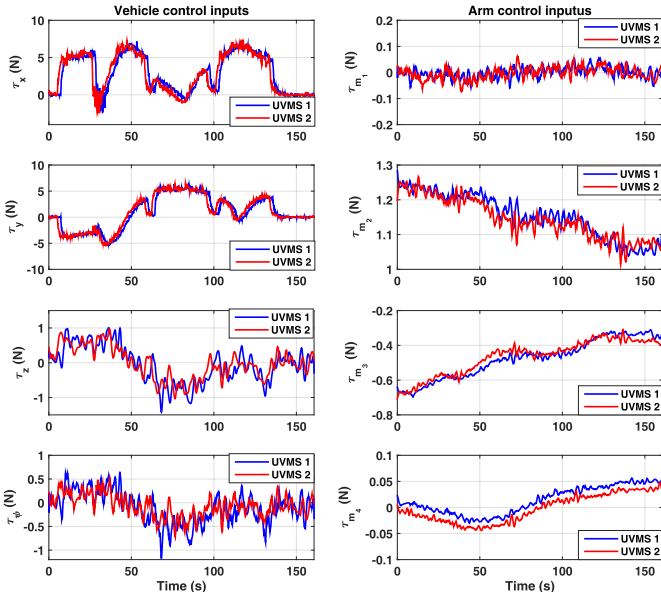


Fig. 9. Simulation study: the control input signals during the control operation

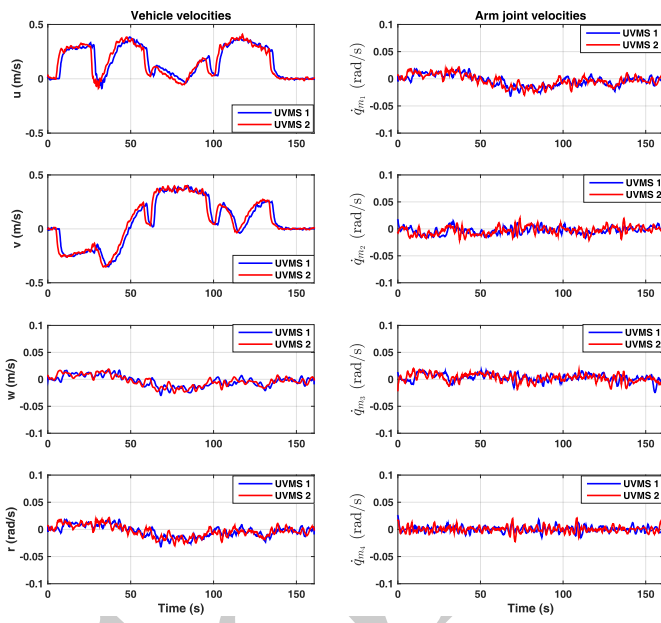


Fig. 10. Simulation study: the evolution of the system velocities at joint level

consider that the vehicle's velocity must not exceed $0.5m/s$ for translation and $0.1rad/s$ for rotational. In the same vein the manipulator joint velocities must be retained between $(-0.1, 0.1)rad/s$. Moreover, the manipulator joint positions (30) must be retained between $(-2, 2)rad$. Furthermore, input saturations (31) for the vehicle and manipulator are considered as: $\bar{v} = 10N$ and $\bar{m} = 2N$, respectively. The sampling time (25) and the prediction horizon are $h = 0.12sec$ and $T_p = 5 \times h = 0.6sec$ respectively. The matrices P_x, Q_x, Q_v and R as well as the load sharing coefficients c_1 and c_2 for both UVMSs are equal and set to: $P_x = Q_x = 0.8 \cdot I_{6 \times 6}$, $R = 0.3 \cdot I_{8 \times 8}$, $Q_v = 0.4 \cdot I_{6 \times 6}$, and $c_1 = c_2 = 0.5$. The initial position of

the object is $x_O = [-0.7, 0, 0.72, 0.04, -0.07, 0]$. We set 3 waypoints as $x_{O_1}^d = [6, -6, 0.85, 0, 0, 0]$, $x_{O_2}^d = [7.5, 1.5, 0.78, 0, 0, 0]$ and $x_{O_3}^d = [12, 6.5, 0.65, 0, 0, 0]$ which make the mission more challenging considering the obstacles' positions within the workspace (See Fig.5 and Fig.4). The results are presented in Fig.5-Fig.7. The trajectory of the system within the workspace as well as the object coordinates evolution are depicted in Fig. 5 and Fig.6 respectively. It can be seen that the UVMSs have successfully transported cooperatively the object and have followed the set of predefined way points while safely avoided the obstacles. The evolution of $\det(J(q)[J(q)^\top])$ (see (4) and (28)) during the operation is given in Fig.7. It can be easily seen that value remained positive during the cooperative manipulation task. Moreover, the evolution of the system velocity and its states at joints level as well as the corresponding control inputs are indicated in Fig.10, Fig. 8 and Fig.9 respectively. As it was expected from the theoretical findings, these values were retained in the corresponding feasible regions defined by the corresponding upper bounds and consequently all of the system constraints were satisfied.

B. Experimental Study

This section demonstrates the efficacy of the proposed cooperative control scheme via a set of real-time experiments employing two small UVMSs equipped with in-house built underwater manipulators, carrying a common object (see Fig. 1). In particular, Subsection IV-B1 introduces the experimental setup and Subsection IV-B2 presents the detailed results of two cases of experimental studies employing the proposed controller.

1) Experimental Setup: The experiments were carried out inside the NTUA, *Control Systems Lab* test tank, with dimensions $5m \times 3m \times 1.5m$ (Fig. 11). The bottom of the tank is covered by a custom-made poster with various visual features and markers. In the following experiments, the team of UVMSs consists of two small ROVs equipped with the same custom made small waterproof manipulator (see Fig.11). More specifically, a 4 DoFs Seabotix LBV (red color), actuated in Surge, Sway, Heave and Yaw and a 3 DoFs VideoRay PRO (yellow color) effective only in Surge, Heave and Yaw motion were used as the vehicle bases in this work (see Fig. 11). Notice that the 3 Dofs VideoRay robot is under-actuated along the Sway axis. This intuitively means that while the combined vehicle-manipulator system is full-actuated at the end-effector frame, the vehicle base remains underactuated along the Sway body frame axis. Thanks to the nature of the optimization procedure, the aforementioned difficulty is handled within the FHOCP (32a)-(32h), which results in a solution that combines the optimal vehicle and manipulator motion in order to achieve the desired movement at the end effector frame. Both of the underwater vehicles are equipped with the same custom made small waterproof manipulator (see Fig. 12). The design parameters of the manipulators are given in Tables I-II. Finally, the object of interest was a pipe whose geometric parameters are given in Table-III.

Both UVMSs are equipped with a down-looking Sony PlayStation Eye camera, with 640×480 pixels at 30 frames



Fig. 11. Experimental setup: custom made UVMSs during real time experiment cooperative transportation. The vehicles used in this work were a 4 DoFs Seabotix LBV and a 3 DoFs VideoRay PRO presented in red and yellow color respectively.

TABLE I
DENAVIT-HARTENBERG PARAMETERS OF THE ROBOTIC ARM

Link	d_i	θ_i	a_i	α_i
1	L_1	q_1	0	$-\frac{\pi}{2}$
2	0	$q_2 - \frac{\pi}{2}$	L_2	0
3	0	$q_3 + \frac{\pi}{2}$	$-L_3$	$\frac{\pi}{2}$
4	L_4	q_4	0	0

TABLE II
PARAMETERS OF THE ROBOTIC ARM

Parameter	Value	Unit
Link 1 Length(L_1)	0.077	m
Link 2 Length(L_2)	0.147	m
Link 3 Length(L_3)	0.028	m
Link 4 Length(L_4)	0.075	m
Link 1 Mass	0.1	kg
Link 2 Mass	0.2	kg
Link 3 Mass	0.1	kg
Link 4 Mass	0.12	kg
Link Diameter	0.06	m

TABLE III
OBJECT CHARACTERISTICS

Parameter	Value	Unit
Length	1.0	m
Pipe Diameter	0.32	m
Mass in Air	0.350	kg

per second (fps) enclosed in a waterproof housing. An underwater laser pointer projecting a green dot at the bottom of the test tank is rigidly attached on the vehicle with its axes aligned to the down-looking camera axis. The visual projection of the laser pointer dot on the image plane, along with various data from vehicle's onboard navigation system sensors (e.g., IMU) are used within a proper sensor fusion algorithm, in order to provide the vehicle state vectors. The Seabotix LBV and the VideoRay PRO are also equipped with *SBG IG-500A AHRS* and 10 DOF IMU Sensor respectively, delivering temperature-compensated 3D acceleration, angular velocity and orientation measurements at 100Hz. The marker localization system is based on the *ArUco* library [54]. For both UVMSs, the complete state vector of the vehicle (3D position, orientation, velocity) as well as the vehicle's dynamic parameters in the following experimental studies are available via the sensor fusion and state estimation module based on the Complementary Filter notion and a proper identification scheme presented in our previous results [52]. The analysis of

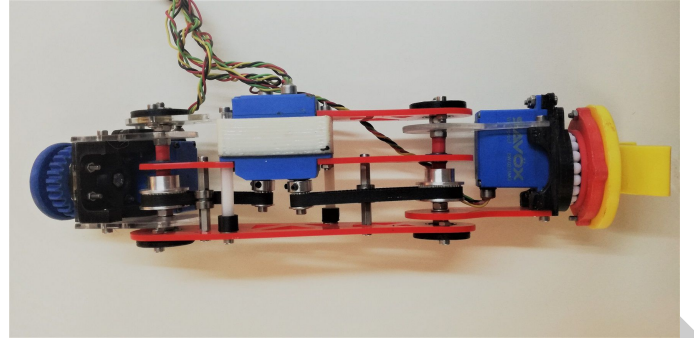


Fig. 12. Custom made 4 Dofs waterproof robotic manipulator used in experimental study.

the sensor fusion, state estimation and parameter identification algorithms are out of the scope of this work and thus omitted. However, they can be found in detail in [52]. The software implementation of the proposed control scheme was conducted in C++ and Python under the Robot Operating System (ROS) [51]. Moreover, the Nonlinear Model Predictive Controller employed in this work was implemented using the NLOpt Optimization library [53] and the overall software was running on two laptops (each UVMS was connected to a separate laptop) with 8 cores, 2.80 GHz CPU and 16 GB of RAM.

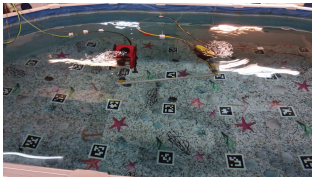
2) *Experimental Results:* In order to prove the efficiency of the proposed controller, two experimental sessions are presented, namely Session A and B. In Session A the objective for the team of UVMSs is to stabilize the object cooperatively in a desired configuration within the test tank while the objective in Session B is to follow a set of predefined waypoints while collaboratively carrying the object. Moreover, in the following experiments the team of UVMS should simultaneously avoid the workspace (test tank) boundaries which were modeled according to the spherical world representation. Notice that the small and limited size of the available test tank, did not allow us to consider obstacles inside the workspace. However, collision avoidance with the test tank boundaries, demonstrates the efficacy of the proposed scheme for avoiding collisions in a real time manner. The radius of the sphere $B(\mathbf{p}_i, \bar{r})$ which covers all the UVMS volume (i.e., main body of the vehicle, additional equipment and robotic manipulator for all possible configurations) is defined as $\bar{r} = 0.75m$. Moreover, the radius of the sphere $B(\mathbf{x}_O, r_O)$ that covers the object is defined as $r_O = 0.5m$ (see Table III). Similar to the simulation part, the Navigation function (23)-(24) was designed with gain $K_{NF} = 0.1$. Regarding to constraints (29), in both experiments, we consider that the vehicle's velocity must not exceed $0.5m/s$ for translation and $0.5rad/s$ for rotational velocities. In the same vein, the manipulator joint velocities must be retained between $(-0.2, 0.2)rad/s$. Moreover, the manipulator joint positions (30) must be retained between $(-2.5, 2.5)rad$ for the first joint q_{m_1} , $(-1.5, 0.7)rad$ for the second joint q_{m_2} , and $(-0.5, 1.5)rad$ for the third joint q_{m_3} , respectively. Notice that the fourth joint q_{m_4} is limit free and thus no joint limit constraints considered to this joint. Furthermore, input saturations (31) for the



(a)



(b)



(c)



(d)

Fig. 13. Experimental study - stabilization scenario: The evolution of the proposed methodology in 4 consecutive time instants.

vehicle and manipulator are considered as: $\bar{\tau}_v = 2N$ and $\bar{\tau}_m = 0.2N$, respectively. The sampling time (25) and the prediction horizon for both of the following experiments are $h = 0.15\text{sec}$ and $T_p = 5 \times h = 0.75\text{sec}$ respectively. Moreover, the matrices P_x , Q_x , Q_v and R as well as the load sharing coefficients c_1 and c_2 for both UVMSs are equal and set to: $P_x = Q_x = 0.5 \cdot I_{6 \times 6}$, $R = 0.15 \cdot I_{8 \times 8}$, $Q_v = 0.2 \cdot I_{6 \times 6}$, and $c_1 = c_2 = 0.5$.

Session A: Stabilization

As stated before, the objective for the team of UVMS in the first experiment is to transfer and stabilize the object into a desired configuration inside the small test tank. More specifically, the desired configuration was set as $x_O^d = [0.0, 0.0, 0.4, 0, 0.45, 1.57]$. The results are presented in Fig.13-Fig.17. The trajectory of the system within the workspace as well as the object coordinates evolution are depicted in Fig. 13 and Fig.14 respectively. It can be seen that the team of UVMSs have successfully transported and stabilized the object to the desired configuration. The evolution of the system velocity at joints level as well as the corresponding control inputs are indicated in Fig.15 and Fig.16, respectively. Moreover, the evolution of the system's velocities is given in Fig.17. It can be seen easily that all of the aforementioned values remained in their corresponding constraints sets during the experiment's evolution.

Session B: Waypoint following

In the following experiment, the objective for the team of UVMSs is to follow a set of predefined waypoints within the workspace while collaboratively carrying the object. More specifically, 4 waypoints were set as given in Table-IV, which make the mission more challenging regarding the stabilization scenario. The results are presented in Fig.18-Fig.21. The object coordinates evolution is depicted in Fig. 19. It can be seen that the UVMSs have successfully transported cooperatively the object and have followed the set of predefined waypoints while safely avoided any collision with the test tank

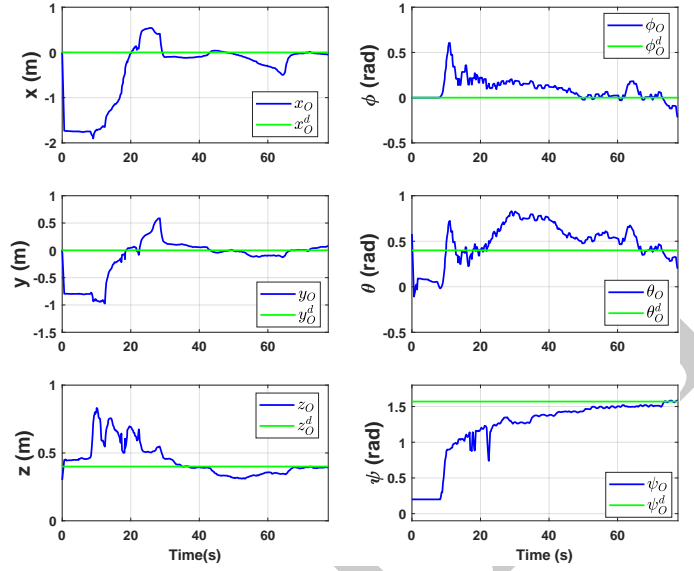


Fig. 14. Experimental study - stabilization scenario: Object coordinates during the control operation

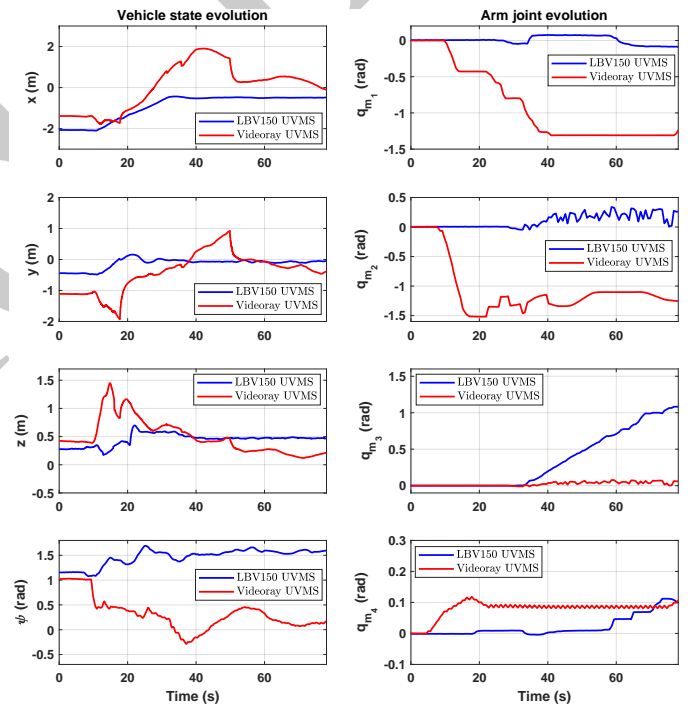


Fig. 15. Experimental study - stabilization scenario: The evolution of the system states at joint level

boundaries. The evolution of the system states and velocities at joints level as well as the corresponding control inputs are indicated in Fig.20 Fig.21 and Fig.22, respectively. As it was expected from the theoretical findings, in both of the considered scenarios, all of the system values were retained in the corresponding constraints sets defined by the respective bounds and consequently all of the system constraints were satisfied.

TABLE IV
THE SET OF PREDEFINED WAYPOINTS

Waypoint	Predefined values for each elements					
	x_O^d	y_O^d	z_O^d	ϕ_O^d	θ_O^d	ψ_O^d
$x_{O_1}^d$	0.0	0.0	0.4	0.0	0.45	1.5
$x_{O_2}^d$	1	0.5	0.4	0.0	0.45	0.0
$x_{O_3}^d$	-0.7	-0.5	0.4	0.0	0.45	0.75
$x_{O_4}^d$	0.0	0.0	0.4	0.0	0.45	1.5

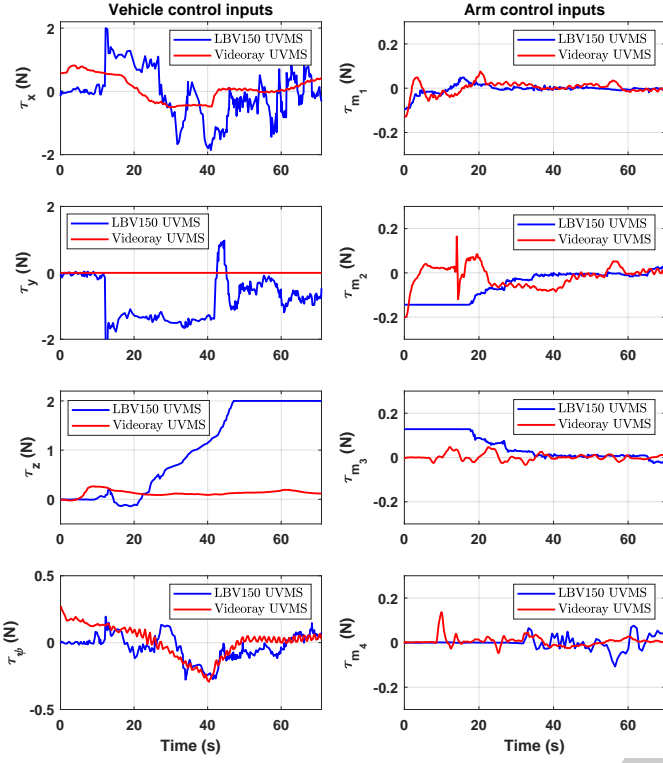


Fig. 16. Experimental study - stabilization scenario: The control input signals during the control operation

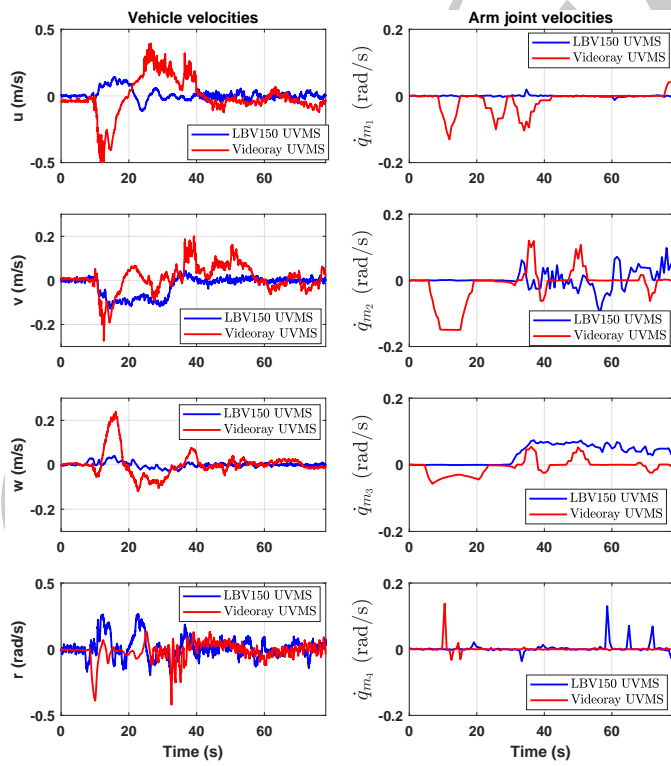


Fig. 17. Experimental study- stabilization scenario: The evolution of the system velocities at joint level

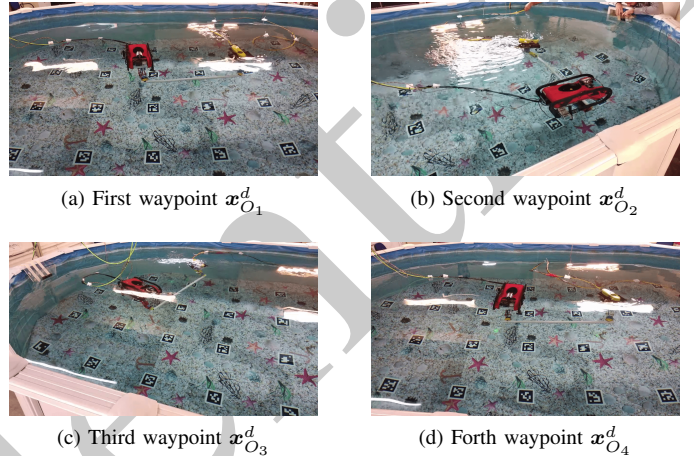


Fig. 18. Experimental study - Waypoint tracking scenario: The evolution of the proposed methodology in 4 consecutive time instants.

C. Video

Two videos demonstrating the aforementioned realistic simulation and the experimental results of the proposed methodology can be found in at the following urls:

- Simulation: <https://youtu.be/O5WHov7EGMI>
- Experiment: <https://youtu.be/eIu57Ftxb1g>

V. SUMMARY AND FUTURE WORK

In this work, we presented a novel distributed object transportation control scheme for a team UVMSs operating in a constrained workspace with static obstacles. Various limits and constraints such as: obstacles, joint limits, control input saturation as well as kinematic and representation singularities have been considered during the control design. The proposed control strategy relieves the team of robots from intense inter-robot communication during the execution of the collaborative tasks hence reducing the need for high bandwidth requirements during explicit information exchange (e.g via acoustic modems). Moreover, the control scheme adopts load sharing among the UVMSs according to their specific payload capabilities. Future research efforts will be devoted towards investigating collaborative grasping and transportation strategies for objects with increased geometric complexity, identifying the optimal regions for safe grasp (e.g no slippage) while taking into account how these regions will affect the manipulability of the augmented (UVMSs and object) system during transportation tasks.

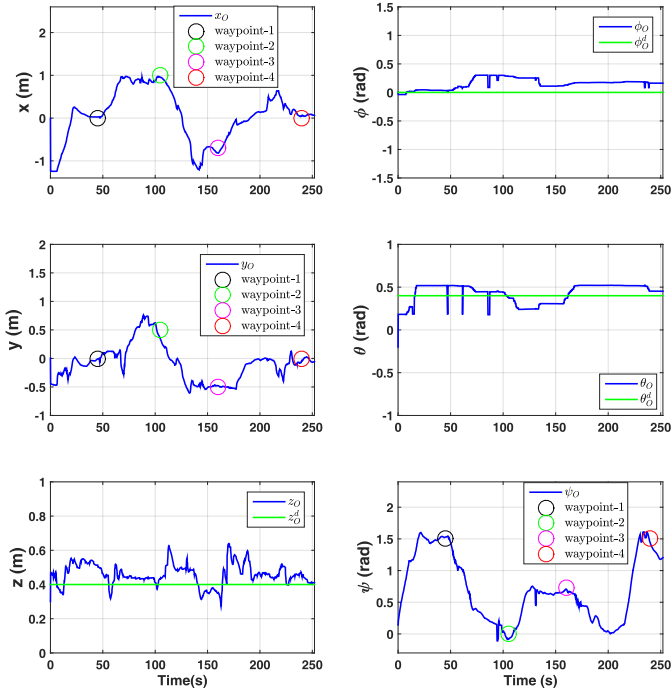


Fig. 19. Experimental study - Waypoint tracking scenario: Object coordinates during the control operation

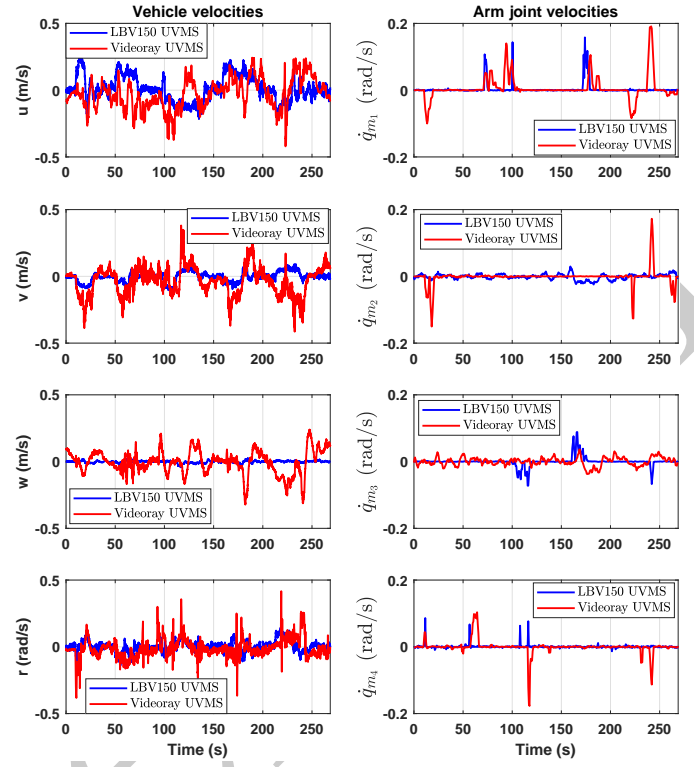


Fig. 21. Experimental study - Waypoint tracking scenario: The evolution of the system velocities at joint level

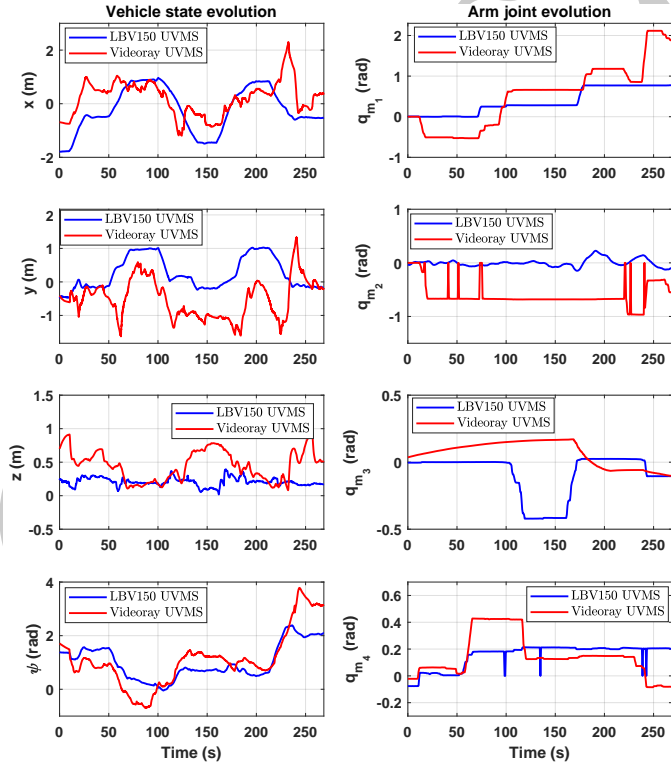


Fig. 20. Experimental study - Waypoint tracking scenario: The evolution of the system states at joint level

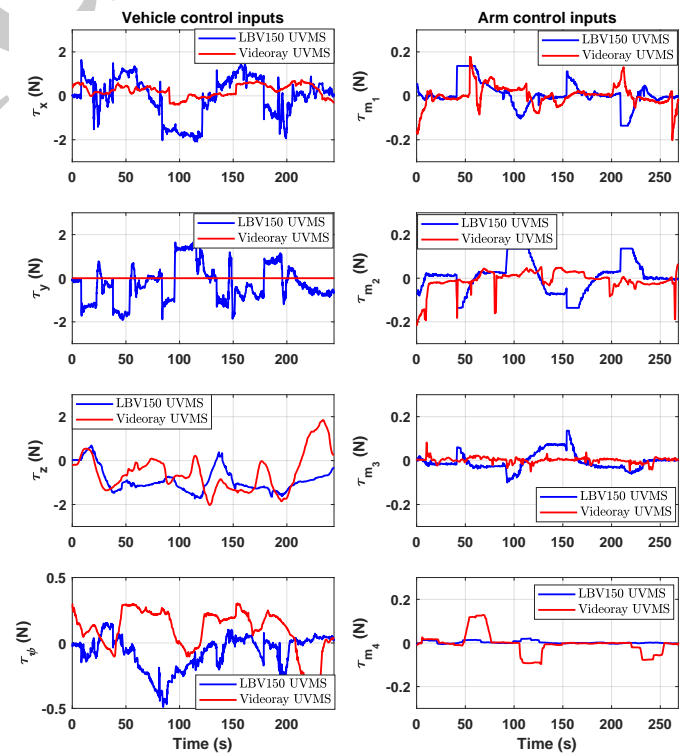


Fig. 22. Experimental study - Waypoint tracking scenario: The control input signals during the control operation

REFERENCES

- [1] T. Fossen, "Guidance and control of ocean vehicles," Wiley, New York, 1994.
- [2] P. Ridao, M. Carreras, D. Ribas, P. Sanz, and G. Oliver, "Intervention auvs: The next challenge," *Annual Reviews in Control*, vol. 40, pp. 227–241, 2015.
- [3] H. Farivarnejad and S. Moosavian, "Multiple impedance control for object manipulation by a dual arm underwater vehicle-manipulator system," *Ocean Engineering*, vol. 89, pp. 82–98, 2014.
- [4] H. Shim, B.-H. Jun, P.-M. Lee, H. Baek, and J. Lee, "Workspace control system of underwater tele-operated manipulators on an rov," *Ocean Engineering*, vol. 37, no. 11-12, pp. 1036–1047, 2010.
- [5] P. Londhe, S. Mohan, B. Patre, and L. Waghmare, "Robust task-space control of an autonomous underwater vehicle-manipulator system by pid-like fuzzy control scheme with disturbance estimator," *Ocean Engineering*, vol. 139, pp. 1–13, 2017.
- [6] S. Mohan and J. Kim, "Coordinated motion control in task space of an autonomous underwater vehicle-manipulator system," *Ocean Engineering*, vol. 104, pp. 155–167, 2015.
- [7] G. Marani, S. Choi, and J. Yuh, "Underwater autonomous manipulation for intervention missions auvs," *Ocean Engineering*, vol. 36, no. 1, pp. 15–23, 2009.
- [8] E. Simetti and G. Casalino, "Whole body control of a dual arm underwater vehicle manipulator system," *Annual Reviews in Control*, vol. 40, pp. 191–200, 2015.
- [9] D. Lane, D. O'Brien, M. Pickett, J. Davies, G. Robinson, D. Jones, E. Scott, G. Casalino, G. Bartolini, G. Cannata, A. Ferrara, D. Angelletti, M. Cocco, G. Veruggio, R. Bono, P. Virgili, M. Canals, R. Pallas, E. Gracia, and C. Smith, "Amadeus: Advanced manipulation for deep underwater sampling," *IEEE Robotics and Automation Magazine*, vol. 4, no. 4, pp. 34–45, 1997.
- [10] V. Rigaud, . Coste-Manière, M. Aldon, P. Probert, M. Perrier, P. Rives, D. Simon, D. Lane, J. Kiener, A. Casals, J. Amat, P. Dauchez, and M. Chantler, "Union: Underwater intelligent operation and navigation," *IEEE Robotics and Automation Magazine*, vol. 5, no. 1, pp. 25–34, 1998.
- [11] P. Sanz, P. Ridao, G. Oliver, G. Casalino, C. Insaurralde, C. Silvestre, C. Melchiorri, and A. Tureta, "Trident: Recent improvements about autonomous underwater intervention missions," *IFAC Proceedings Volumes (IFAC-PapersOnline)*, vol. 3, no. PART 1, pp. 355–360, 2012.
- [12] M. Prats, J. Garcia, S. Wirth, D. Ribas, P. Sanz, P. Ridao, N. Gracias, and G. Oliver, "Multipurpose autonomous underwater intervention: A systems integration perspective," *2012 20th Mediterranean Conference on Control and Automation, MED 2012*, pp. 1379–1384, 2012.
- [13] J. Fernández, M. Prats, P. Sanz, J. García, R. Marín, M. Robinson, D. Ribas, and P. Ridao, "Grasping for the seabed: Developing a new underwater robot arm for shallow-water intervention," *IEEE Robotics and Automation Magazine*, vol. 20, no. 4, pp. 121–130, 2013.
- [14] E. Simetti, G. Casalino, S. Torelli, A. Sperindé, and A. Tureta, "Floating underwater manipulation: Developed control methodology and experimental validation within the trident project," *Journal of Field Robotics*, vol. 31, no. 3, pp. 364–385, 2014.
- [15] M. Prats, D. Ribas, N. Palomeras, J. García, V. Nannen, S. Wirth, J. Fernández, J. Beltrán, R. Campos, P. Ridao, P. Sanz, G. Oliver, M. Carreras, N. Gracias, R. Marín, and A. Ortiz, "Reconfigurable auv for intervention missions: A case study on underwater object recovery," *Intelligent Service Robotics*, vol. 5, no. 1, pp. 19–31, 2012.
- [16] D. Ribas, P. Ridao, A. Tureta, C. Melchiorri, G. Palli, J. Fernandez, and P. Sanz, "I-auv mechatronics integration for the trident fp7 project," *IEEE/ASME Transactions on Mechatronics*, vol. 20, no. 5, pp. 2583–2592, 2015.
- [17] D. Lane, F. Maurelli, P. Kormushev, M. Carreras, M. Fox, and K. Kyriakopoulos, "Persistent autonomy: The challenges of the pandora project," *IFAC Proceedings Volumes (IFAC-PapersOnline)*, vol. 9, no. PART 1, pp. 268–273, 2012.
- [18] A. Carrera, N. Palomeras, D. Ribas, P. Kormushev, and M. Carreras, "An intervention-auv learns how to perform an underwater valve turning," *OCEANS 2014 - TAIPEI*, 2014.
- [19] A. Carrera, N. Palomeras, N. Hurtos, P. Kormushev, and M. Carreras, "Learning multiple strategies to perform a valve turning with underwater currents using an i-auv," *MTS/IEEE OCEANS 2015 - Genova: Discovering Sustainable Ocean Energy for a New World*, 2015.
- [20] J. Gancet, D. Urbina, P. Letier, M. Ilzokvitz, P. Weiss, F. Gauch, G. Antonelli, G. Indiveri, G. Casalino, A. Birk, M. Pfingsthorn, S. Calinon, A. Tanwani, A. Tureta, C. Walen, and L. Guipain, "Dexrov: Dexterous undersea inspection and maintenance in presence of communication latencies," *IFAC-PapersOnLine*, vol. 28, no. 2, pp. 218–223, 2015.
- [21] T. Padir and A. Koivo, "Modeling of two underwater vehicles with manipulators on-board," *In Proceedings of the IEEE International Conference on Systems, Man and Cybernetics*, vol. 2, pp. 1359–1364, 2003.
- [22] Y. Sun and C. Cheah, "Coordinated control of multiple cooperative underwater vehicle-manipulator systems holding a common load," *In Proceedings of the IEEE Techno-Ocean '04: Bridges across the Oceans*, vol. 3, pp. 1542–1547, 2004.
- [23] N. McClamroch, "Singular systems of differential equations as dynamic models for constrained robot systems," *In Proceedings of the IEEE International Conference on Robotics and Automation*, pp. 21–28, 1986.
- [24] T. Padir, "Kinematic redundancy resolution for two cooperating underwater vehicles with on-board manipulators," *In Proceedings of the IEEE International Conference on Systems, Man and Cybernetics*, pp. 3137–3142, 2005.
- [25] T. Padir and J. Nolff, "Manipulability and maneuverability ellipsoids for two cooperating underwater vehicles with on-board manipulators," *In Proceedings of the IEEE International Conference on Systems, Man and Cybernetics*, pp. 3656–3661, 2007.
- [26] R. Cui, S. Ge, B. Voon Ee How, and Y. Sang Choo, "Leader-follower formation control of underactuated autonomous underwater vehicles," *Ocean Engineering*, vol. 37, no. 17-18, pp. 1491–1502, 2010.
- [27] D. J. Stilwell and B. E. Bishop, "Framework for decentralized control of autonomous vehicles," *In Proceedings of the IEEE International Conference on Robotics and Automation*, vol. 3, pp. 2358–2363, 2000.
- [28] M. Uchiyama and P. Dauchez, "Symmetric hybrid position/force control scheme for the coordination of two robots," *In Proceedings of the IEEE International Conference on Robotics and Automation*, pp. 350–356, 1988.
- [29] O. Khatib, "Object manipulation in a multi-effector robot system," *in proceeding of the 4th International Symposium on Robotic Research*, vol. 4, pp. 137–144, 1988.
- [30] H. Tanner, S. Loizou, and K. Kyriakopoulos, "Nonholonomic navigation and control of cooperating mobile manipulators," *IEEE Transactions on Robotics and Automation*, vol. 19, no. 1, pp. 53–64, 2003.
- [31] S. Schneider and J. Cannon, R.H., "Object impedance control for cooperative manipulation: Theory and experimental results," *IEEE Transactions on Robotics and Automation*, vol. 8, no. 3, pp. 383–394, 1992.
- [32] C. K. Verginis, A. Nikou, and D. V. Dimarogonas, "Communication-based decentralized cooperative object transportation using nonlinear model predictive control," *in 2018 European Control Conference (ECC)*, pp. 733–738, IEEE, 2018.
- [33] R. Conti, E. Meli, A. Ridolfi, and B. Allotta, "An innovative decentralized strategy for i-auvs cooperative manipulation tasks," *Robotics and Autonomous Systems*, vol. 72, pp. 261–276, 2015.
- [34] R. Furferi, R. Conti, E. Meli, and A. Ridolfi, "Optimization of potential field method parameters through networks for swarm cooperative manipulation tasks," *International Journal of Advanced Robotic Systems*, vol. 13, no. 5, pp. 1–13, 2016.
- [35] E. Simetti and G. Casalino, "Manipulation and transportation with cooperative underwater vehicle manipulator systems," *IEEE Journal of Oceanic Engineering*, 2016.
- [36] N. Manerikar, G. Casalino, E. Simetti, S. Torelli, and A. Sperindé, "On autonomous cooperative underwater floating manipulation systems," *In Proceedings of the IEEE International Conference on Robotics and Automation*, vol. 2015-June, 2015.
- [37] N. Manerikar, G. Casalino, E. Simetti, S. Torelli, and A. Sperindé, "On cooperation between autonomous underwater floating manipulation systems," *2015 IEEE Underwater Technology, UT 2015*, 2015.
- [38] E. Simetti and G. Casalino, "A novel practical technique to integrate inequality control objectives and task transitions in priority based control," *Journal of Intelligent and Robotic Systems: Theory and Applications*, vol. 84, no. 1-4, pp. 877–902, 2016.
- [39] J. Gudiño-Lau, M. A. Arteaga, L. A. Munoz, and V. Parra-Vega, "On the control of cooperative robots without velocity measurements," *IEEE Transactions on Control Systems Technology*, vol. 12, no. 4, pp. 600–608, 2004.
- [40] F. Caccavale, P. Chiacchio, and S. Chiaverini, "Task-space regulation of cooperative manipulators," *Automatica*, vol. 36, no. 6, pp. 879–887, 2000.
- [41] H. Farivarnejad and S. A. A. Moosavian, "Multiple impedance control for object manipulation by a dual arm underwater vehicle–manipulator system," *Ocean Engineering*, vol. 89, pp. 82–98, 2014.
- [42] S. A. A. Moosavian and E. Papadopoulos, "Multiple impedance control for object manipulation," *in Intelligent Robots and Systems, 1998. Proceedings., 1998 IEEE/RSJ International Conference on*, vol. 1, pp. 461–466, IEEE, 1998.

- [43] S. A. A. Moosavian and E. Papadopoulos, "Cooperative object manipulation with contact impact using multiple impedance control," *International Journal of Control, Automation and Systems*, vol. 8, no. 2, pp. 314–327, 2010.
- [44] F. Allgöwer, R. Findeisen, and Z. Nagy, "Nonlinear model predictive control: From theory to application," *the Chinese Institute of Chemical Engineers*, vol. 35, no. 3, pp. 299–315, 2004.
- [45] D. Koditschek and E. Rimon, "Robot navigation functions on manifolds with boundary," *Advances in Applied Mathematics*, vol. 11, no. 4, pp. 412–442, 1990.
- [46] G. Antonelli, "*Underwater Robots*". Springer Tracts in Advanced Robotics, Springer International Publishing, 2013.
- [47] B. Siciliano, L. Sciavicco, and L. Villani, *Robotics : modelling, planning and control*. Advanced Textbooks in Control and Signal Processing, Springer, 2009. 013-81159.
- [48] S. Soylu, B. Buckham, and R. Podhorodeski, "Redundancy resolution for underwater mobile manipulators," *Ocean Engineering*, vol. 37, no. 2-3, pp. 325–343, 2010.
- [49] S. Heshmati-Alamdari, G. C. Karras, P. Marantos, and K. J. Kyriakopoulos, "A robust model predictive control approach for autonomous underwater vehicles operating in a constrained workspace," *In Proceedings of the IEEE International Conference on Robotics and Automation, ICRA*, 2018.
- [50] M. Prats, J. Perez, J. Fernandez, and P. Sanz, "An open source tool for simulation and supervision of underwater intervention missions," in *IEEE/RSJ International Conference on Intelligent Robots and Systems (IROS)*, pp. 2577–2582, 2012.
- [51] M. Quigley, B. Gerkey, K. Conley, J. Faust, T. Foote, J. Leibs, E. Berger, R. Wheeler, and A. Ng, "Ros: an open-source robot operating system," in *Proc. of the IEEE Intl. Conf. on Robotics and Automation (ICRA) Workshop on Open Source Robotics*, (Kobe, Japan), May 2009.
- [52] G. C. Karras, P. Marantos, C. P. Bechlioulis, and K. J. Kyriakopoulos, "Unsupervised online system identification for underwater robotic vehicles," *IEEE Journal of Oceanic Engineering*, 2018.
- [53] S. G. Johnson, "The nlopt nonlinear-optimization package," <http://ab-initio.mit.edu/nlopt>.
- [54] S. Garrido-Jurado, R. M. noz Salinas, F. Madrid-Cuevas, and M. Marín-Jiménez, "Automatic generation and detection of highly reliable fiducial markers under occlusion," *Pattern Recognition*, vol. 47, no. 6, pp. 2280 – 2292, 2014.